JUN 1 0 1970
JUL 1 ? 1970

AEDC-TR-70-23

Copy 2

RESOLUTION LIMITS OF FRAUNHOFER HOLOGRAPHY

Ronald A. Belz

ARO, Inc.

May 1970

This document has been approved for public release and sale; its distribution is unlimited.

ARNOLD ENGINEERING DEVELOPMENT CENTER
AIR FORCE SYSTEMS COMMAND
ARNOLD AIR FORCE STATION, TENNESSEE

PROPERTY OF U. S. AIR FORCE
AEDC LIBRARY
F40600 - 69 - C - 0001

NOTICES

When U. S. Government drawings specifications, or other data are used for any purpose other than a definitely related Government procurement operation, the Government thereby incurs no responsibility nor any obligation whatsoever, and the fact that the Government may have formulated, furnished, or in any way supplied the said drawings, specifications, or other data, is not to be regarded by implication or otherwise, or in any manner licensing the holder or any other person or corporation, or conveying any rights or permission to manufacture, use, or sell any patented invention that may in any way be related thereto.

Qualified users may obtain copies of this report from the Defense Documentation Center.

References to named commercial products in this report are not to be considered in any sense as an endorsement of the product by the United States Air Force or the Government.

RESOLUTION LIMITS OF FRAUNHOFER HOLOGRAPHY

Ronald A. Belz*
ARO, Inc.

This document has been approved for public release and sale; its distribution is unlimited.

*Research Assistant, ARO, Inc., and student at The University of Tennessee Space Institute, Tullahoma, Tennessee.

FOREWORD

The work reported herein was sponsored by the Arnold Engineering Development Center (AEDC), Air Force Systems Command (AFSC), under Program Elements 64719F and 62201F, Project 4344, Task 32.

The results of research were obtained by ARO, Inc. (a subsidiary of Sverdrup & Parcel and Associates, Inc.), contract operator of AEDC, AFSC, Arnold Air Force Station, Tennessee, under Contract F40600-69-C-0001 and under ARO, Inc., Subcontract 70-20/TS-OMD with the University of Tennessee Space Institute (UTSI), Tullahoma, Tennessee. The work was performed between June and September, 1969, under ARO Project No. BC5016, and the manuscript was submitted for publication on December 19, 1969.

This report describes work performed by the author for ARO, Inc., Technical Staff, Experimental Research, while assigned as a research assistant to ARO, Inc., by UTSI. Messrs. M. L. Frame and H. N. Glassman of the Central Computer Organization of ARO, Inc., are acknowledged for their assistance with the computer program.

This technical report has been reviewed and is approved.

David G. Francis
1Lt, USAF
Research Division
Directorate of Plans
and Technology

Harry L. Maynard
Colonel, USAF
Director of Plans
and Technology

ABSTRACT

The resolution of an in-line hologram recorded with plane waves in the Fraunhofer region of a circular, opaque, particle is evaluated. From the diffraction integral for the reconstructed, real image the intensity distribution about the image is found. Criteria for determining the edge of the image in addition to determining the plane of focus are specified from the data, and the measurement accuracies are found. The inaccuracies are shown to be a result of the inability of the film to record all of the light diffracted by the particle. The reasons for this, film grain noise and its cutoff frequency and dynamic range, are explained and their relative effects compared for the various particle sizes and recording distances.

CONTENTS

		Page
	ABSTRACT	iii
	NOMENCLATURE	vii
I.	INTRODUCTION	
	1.1 Problem Statement	1
	1.2 In-Line Holography and Its Application to Instrumen-	1
	tation	1
II.	THEORETICAL ANALYSIS	
	2.1 Derivation of the Focusing Integral	3
	2.2 Special Cases of the Focusing Integral	10
	2.3 Data from the Focusing Integral	14
	2.4 Validity of Scalar Diffraction Theory	15
III.	THEORETICAL RESOLUTION	
	3.1 Particle Position	16
	3.2 Limiting Parameters of the Film	20
IV.	SUMMARY AND CONCLUSIONS	25
	REFERENCES	28

APPENDIXES

I. ILLUSTRATIONS

Figure		
1.	Hologram Recording and Reconstruction with Spherical Waves	33
2.	Intensity at the Edge of the Particle Image	34
3.	Normalized Intensity at the Edge of the Particle Image	35
4.	Slope at the Edge of the Particle Image	36
5.	Normalized Slope at the Particle Image Edge	37
6.	Normalized Intensity Distribution along the Optic Axis	38
7.	Isophote Diagram	39
8.	Isophote Diagram	40
9.	Isophote Diagram	41

Figure		Page
10.	Isophote Diagram	42
11.	Isophote Diagram	43
12.	Intensity Variation Perpendicular to the Optic Axis for Various Values of n	44
13.	Intensity Variation Perpendicular to the Optic Axis for Various Values of n	45
14.	Intensity Variation Perpendicular to the Optic Axis for Various Values of n	46
15.	Intensity Variation Perpendicular to the Optic Axis for Various Values of n	47
16.	Intensity Variation Perpendicular to the Optic Axis for Various Values of n	48
17.	Intensity Variation at the Center and Edge of the Particle Image as it is Brought into and out of Focus	49
18.	Intensity Variation at the Center and Edge of the Particle Image as it is Brought into and out of Focus	50
19.	Intensity Variation at the Center and Edge of the Particle Image as it is Brought into and out of Focus	51
20.	Intensity Variation at the Center and Edge of the Particle Image as it is Brought into and out of Focus	52
21.	Intensity Variation at the Center and Edge of the Particle Image as it is Brought into and out of Focus	53
22.	The Diffraction Pattern Resulting from Plane Wave Illumination of a Circular, Opaque Particle	54
23.	Peaks of $J_1(\Omega)/\Omega$ versus Ω for the Signal-to-Noise Ratio Calculation	55

II. TABLES

I.	Theoretical Error in the Particle Radius, When the Intensity is 25 percent of that at the Center of the Image	56
II.	Maximum Theoretical Error in the Particle Radius Measurement Arising from Measuring the Outermost Peak on the Image	56

Page

II. TABLES (Continued)

III. Focal Tolerance Constant, $K(\Omega)$, for a Hologram and a Thin-Lens 57

IV. Maximum Limiting Aperture Radii and Maximum Arguments of $J_1(\Omega)$ for ν_{max} = 200 Lines/mm 58

V. Maximum Limiting Aperture Radii and Maximum Arguments of $J_1(\Omega)$ for the Diffraction Pattern Recording Limited by Film Noise 59

III. COMPUTER PROGRAM FOR THE FOCUSING INTEGRAL 60

NOMENCLATURE

a	Particle radius
c	$\frac{k_2{}^2 a}{2\pi z_2}$
D	$\frac{k_1 a}{z_1}$
$\bar{D}$	Photographic density
$D(\bar{r})$	Amplitude transmission coefficient
F/#	Hologram "F" number; the focal length over the effective hologram diameter
H	The radius of the effective hologram aperture
I	Intensity
i	$\sqrt{-1}$
J_i	The ith- order Bessel function
k_1	Recording wave number
k_2	Reconstruction wave number
N	Far-field number
R_2	Distance from reconstruction point source to hologram
r	Radial distance in recording plane

s	Source plane position during recording
s'	Source plane position during reconstruction
SNR	Signal-to-noise ratio
u	$\frac{k_2}{z_2} - \frac{k_1}{z_1}$
v	$\frac{k_2 w}{z_2}$
$\overline{w}$	Position vector referenced to reconstruction plane
z_o	Radius of curvature of illuminating wave
z_1	Distance from particle to hologram
z_2	Reconstruction distance from hologram
γ	Photographic contrast coefficient
η	Distance measured from geometrical focus
λ_1	Recording wavelength
λ_2	Reconstruction wavelength
θ	Angular coordinate in hologram plane
ν	Film frequency
σ	Film noise
ϕ	Angular coordinate in reconstruction plane
ψ_{real}	Real wavefront potential
$\psi_{virtual}$	Virtual wavefront potential
Ω	Argument of the first-order Bessel function

SECTION I
INTRODUCTION

1.1 PROBLEM STATEMENT

In-line, Fraunhofer holography is a convenient means of recording and measuring particle size, position, and velocity in a dynamic volume. Over the past few years it has been used in aerosol studies to measure the size distribution and velocity of the particle droplets (Refs. 1, 2, and 3). These studies have brought out the need to know the limiting accuracy for measuring the size and position of the reconstructed images. The accuracy of these measurements is important especially for the velocity data where the ability to bring an image into focus and determine its exact position from the hologram is essential. The factors which limit this accuracy must also be known so that the hologram recording may be improved to yield more accurately reconstructed images. The errors inherent in measuring the particle image size and finding the planes in which the reconstructed images are in focus should, therefore, be determined analytically.

1.2 IN-LINE HOLOGRAPHY AND ITS APPLICATION TO INSTRUMENTATION

There are two basic ways of recording a hologram: (1) in line and (2) off axis. The simplest, and historically the first, is the in-line hologram. It is formed by illuminating a volume consisting of particles with a coherent beam of light. The light diffracted by the particles interferes with the undiffracted portion producing an intensity variation which contains both the phase and amplitude information of the light. These intensity variations are recorded as interference patterns on film. The developed negative is a hologram which, when placed into a beam of coherent light, will reconstruct a real and virtual image of the particle field. If plane waves are used to record and reconstruct the hologram, the images are reconstructed exactly to size and position as the original particles were relative to the film. The images are located on either side of the film "in line" with the reconstruction beam. The recording and reconstruction arrangements are illustrated in Fig. 1, Appendix I. The hologram is recorded in the far-field, Fraunhofer region of the particles to keep the two images from interfering during the reconstruction (Ref. 4).

Sizes and positions of the particles in the volume can be determined from the hologram. The velocity of the particles can also be found in two ways. If, during the exposure of the film, the particles move, their reconstructed images will be smeared. (Unlike the other holographic

techniques, motion during the recording is not limited to less than a wavelength.) From the length of this smear and the exposure time the velocity of the particle can be calculated (Ref. 5). The second method of obtaining the velocity is based on doubly exposing the hologram. The holograms taken at two instants of time reconstruct volumes containing similar particles that are displaced in space according to their velocities. Velocities are, therefore, found from the separation of the two particle images and the time separation between exposures (Refs. 3, 6, 7, and 8).

Besides reconstructing the images and measuring their sizes, positions, and velocities in the volume, there are two other methods of reducing these data. The first, and most basic, is by direct analysis of the recorded interference patterns (Refs. 7 and 9). This was used in the preliminary stages of particle field analysis using coherent illumination and has been found to contain a number of shortcomings, making data reduction impractical (Ref. 10). Optical data processing of the hologram, the second method, is as yet in its preliminary stages of development (Ref. 11).

To produce a high quality in-line hologram, the recording must be made in the far-field region of the individual particles. This condition limits the maximum particle size that can be recorded since the Fraunhofer region of particles larger than one millimeter is more than one meter away. Diffraction patterns of particles less than 10 μm are difficult to record because of the small amount of light diffracted. The density of the particles in the volume must not be so large that the reference beam is cut out. Reference 10 gives a plot of the maximum allowable density for a given particle size and volume depth.

The velocity that can be recorded is limited by the pulse width and separation. For nonsmeared reconstructions in the double-pulse technique, the pulse width must be such that the particles move less than a tenth of their diameter. The pulse separation, however, must not be so close that the images cannot be resolved or so far apart that the two images cannot be paired.

The accuracy with which the particle size and velocity data from the reconstructed images of the particles can be measured must be known in order to determine the inherent error of the reconstruction process. The theoretical error involved in an instrumentation readout of these image parameters limits the accuracy of the instrument. The study to be reported here was concerned with the hologram resolution of the particle image and its focal plane. Associated with every hologram is a limiting aperture which affects its resolution capabilities. The causes of the limiting aperture and the resolution capabilities of a given film are shown.

Section II will consist of the derivation of the focusing integral for the image and special cases of this integral which have closed form solutions. In Section III the data from the numerical integration of the focusing integral will be used to define criteria to describe the capability of an instrument in determining the particle image size and location. The limiting criteria are found in terms of the finite size of the recorded interference patterns. The importance of the various causes of the limited size of the patterns are studied.

SECTION II
THEORETICAL ANALYSIS

2.1 DERIVATION OF THE FOCUSING INTEGRAL

An in-line hologram can be recorded with plane or spherical waves. To keep the analysis from being restricted to any special case, the initial derivation for the reconstructed image will be for spherical waves. The point source and recording plane will be in the far-field region of the circular particle where the recording distance, z_1, written in terms of far fields is

$$z_1 \equiv \frac{4a^2N}{\lambda_1} \tag{1}$$

where λ_1 is the wavelength of the illuminating wavefront, N is the far-field number, and a is the particle radius. When this criterion is not met, the film is in the Fresnel region and the reconstructed image suffers from interference with the still large intensity conjugate image. The schematic arrangement for recording the diffraction patterns and reconstructing the images is shown in Fig. 1.

The normalized intensity distribution in the recording plane caused by an opaque, circular particle illuminated with spherical waves of radius z_o is (Ref. 12)

$$I(r) = \frac{1}{(z_o + z_1)^2} + \frac{a^2 J_1^2\left(\frac{k_1 ar}{z_1}\right)}{r^2 z_o^2} - \frac{2\left(\frac{a}{r}\right) J_1\left(\frac{kar}{z_1}\right)}{z_o (z_o + z_1)} \sin\left(\frac{k_1 z_o r^2}{2z_1 (z_o + z_1)}\right) \tag{2}$$

This intensity distribution is the interference between the diverging background light which has been unaffected by the particle and the light scattered by the particle. The first two terms represent a background intensity caused by the reference and object waves and give no information to the reconstructed image. These terms merely represent the

intensity that would be recorded if the particle were illuminated with incoherent light, i.e., interference effects are not present. The third term is, however, a result of the coherent interference and is responsible for forming the reconstructed images. The analysis is greatly simplified if it is assumed that the developed photographic film is characterized by a linear relationship between the exposure intensity and the amplitude transmission coefficient. Although such a relationship rarely exists, the linear terms are at least present in the general expansion relating the two. The assumption of linearity furthermore requires a modulation transfer function of unity, a condition which is never given by photographic materials. The assumption, therefore, represents a "best possible case" limit. The equations hereafter are based on the linearity assumption.

Expanding the sine function yields two terms, ψ real and ψ virtual, the real and virtual focusing terms, respectively, where

$$\psi_{real} = \frac{i\, a^2\, k_1}{z_o\, z_1\, (z_o + z_1)} \frac{J_1\left(\frac{k_1 a r}{z_1}\right)}{\left(\frac{k_1 a r}{z_1}\right)} \exp\left[-i \frac{i\, k_1\, z_o}{2 z_1\, (z_o + z_1)} r^2\right] \tag{3}$$

and

$$\psi_{virtual} = \frac{-i\, a^2\, k_1}{z_o\, z_1\, (z_o + z_1)} \frac{J_1\left(\frac{k_1 a r}{z_1}\right)}{\left(\frac{k_1 a r}{z_1}\right)} \exp\left[\frac{i\, k_1\, z_o}{2 z_1\, (z_o + z_1)} r^2\right] \tag{4}$$

Only the real image term will be used in the following analysis since it can be recorded without lenses. The background and the virtual image term can be ignored as long as the far-field condition (Eq. (1)) is observed.

The light distribution, $\psi(\bar{w})$(Fig. 1), in a plane apart from the hologram, formed by light from the point source s′, which is diffracted by the hologram, is given by the Fresnel-Kirchoff diffraction integral (Ref. 13)

$$\psi(\bar{w}) = c \int_{aperture} \psi_i(\bar{r})\, D(\bar{r}) e \exp\left[i k_2 R(\bar{r}, \bar{w})\right] d\bar{r} \tag{5}$$

where

$$c = \frac{(1 - i\, k_2\, z_2)}{2\pi\, z_2 2} \cos\theta' \approx \frac{-i k_2}{2\pi z_2} \tag{6}$$

(where the paraxial approximation has been used) and

$k_2 = \frac{2\pi}{\lambda_2}$

z_2 = distance from the hologram plane to the observation plane

θ' = the angle between the line joining a point on the hologram to a point in the observation plane and the normal to the hologram ($\cos\theta' = \frac{z_1}{R} \approx 1$)

$\psi_i(\bar{r})$ = light distribution incident on the hologram

$D(\bar{r})$ = amplitude transmittance of the hologram

The light from the point source incident on the hologram is from the quadratic approximation

$$\psi_i(\bar{r}) = -\frac{i\,k_2}{2\pi R_2} \exp(ik_2R_2) \exp\left(\frac{ik_2r^2}{2R_2}\right) \tag{7}$$

where R_2 is the distance from the point source to the hologram plane. Expanding $R(\bar{r}, \bar{w})$ in the Fresnel-Kirchoff integral in a binomial expansion

$$R(\bar{r},\bar{w}) = z_2\left(1 + \frac{|\bar{r}|^2}{2z_2{}^2} + \frac{|\bar{w}|^2}{2z_2{}^2} - \frac{\bar{r}\cdot\bar{w}}{z_2{}^2}\right) \tag{8}$$

and substituting Eqs. (3), (7), and (8) into Eq. (5), the Fresnel-Kirchoff equation yields:

$$\psi(\bar{w},z_2) = K \int_{\substack{\text{hologram}\\ \text{aperture}}} \frac{1}{r} J_1\left(\frac{k_1ar}{z_1}\right) \exp\left[\frac{i\,k_1\,z_o}{2z_1\,(z_o+z_1)}\,r^2\right] \exp\left[i\,\frac{k_2}{2}\left(\frac{1}{R_2} - \frac{1}{z_2}\right)r^2\right] \exp\left(-ik_2\,\frac{\bar{w}\cdot\bar{r}}{z_2}\right) d\bar{r} \tag{9}$$

$$K = \frac{k_2{}^2}{(2\pi)^2\,z_2R_2}\,\frac{a}{z_o\,(z_o+z_1)} \exp(ik_2R_2)\exp(ik_2z_2)\exp\left(\frac{ik_2w^2}{2z_2}\right) \tag{10}$$

($\bar{w}$ and $\bar{r}$ are the cartesian vectors in the reconstruction plane and hologram plane, respectively.) Expanding their dot product in polar coordinates gives

$$\bar{w}\cdot\bar{r} = wr\cos(\theta - \phi)$$

and also

$$d\bar{r} = r\,dr\,d\theta$$

The integral now becomes, after separating the integration over θ from that over r,

$$\psi(\bar{w},z_2) = K \int_0^H J_1\left(\frac{k_1 ar}{z_1}\right) \exp\left[\frac{-i\, k_1\, z_0}{z_1\,(z_0 + z_1)}\, r^2\right] \exp\left[i\, \frac{k_2}{2}\left(\frac{1}{R_2} + \frac{1}{z_2}\right) r^2\right] dr$$

$$\int_0^{2\pi} \exp\left[\frac{ik_2\, wr \cos(\theta - \phi)}{z_2}\right] d\theta \tag{11}$$

Integration along the radial vector, r, has an upper limit, H, corresponding to the limiting aperture of the hologram.

The integral over the angle θ is recognized as being the integral representation of the zeroth-order Bessel function, i.e.,

$$\int_0^{2\pi} \exp\left[\frac{-irw}{2z_2} \cos\,(\theta - \phi)\right] d\theta = 2\pi\, J_0\left(\frac{k_2 rw}{z_2}\right) \tag{12}$$

Therefore,

$$\psi(\dot{w},z_2) = 2\pi K \int_0^H J_1\left(\frac{k_1 ar}{z_1}\right) J_0\left(\frac{k_2 rw}{z_2}\right) \exp\left[\frac{-ik_1 z_0 r^2}{2z_1\,(z_0 + z_1)}\right]$$
$$\exp\left[\frac{k_2}{2}\left(\frac{1}{R_2} + \frac{1}{z_2}\right) r2\right] dr \tag{13}$$

This integral, evaluated, describes the light distribution in a plane z_2 from the hologram. Because it is independent of ϕ, the bar has been left off the w, indicating that it now is a radial vector.

Using Euler's Formula

$$\exp(i\theta) = \cos\theta + i \sin\theta \tag{14}$$

and the fact that

$$I(\bar{w}) = \psi(\bar{w})\ \psi^*(\bar{w}) \tag{15}$$

the intensity in the plane at z_2 is

$$I(w,z_2) = (2\pi)^2\ |K|^2 \left\{\left[\int_0^H J_1\,(Dr)\, J_0\,(vr) \cos\left(\frac{u'}{2}\, r^2\right) dr\right]^2\right.$$
$$\left. + \left[\int_0^H J_1\,(Dr)\, J_0\,(vr) \sin\left(\frac{u'}{2}\, r^2\right) dr\right]^2\right\} \tag{16}$$

where

$$D = \frac{k_1 a}{z_i} \tag{17}$$

$$v = \frac{k_2 w}{z_2} \tag{18}$$

$$u' = k_2\left(\frac{1}{R_2} - \frac{1}{z_2}\right) - \frac{k_1 z_o}{z_1(z_o + z_1)} \tag{19}$$

Before proceeding further to the case of plane wave recording and reconstruction, it will be shown that this equation indeed produces an enlarged image of the particle. Let $u' = 0$ which is the focusing condition for the image and assume the hologram contains all of the diffracted light, i.e., $H = \infty$. Then Eq. (16) becomes

$$I(w,z_2) = (2\pi)^2 \, |K|^2 \left[\int_o^\infty J_1(Dr)\, J_o(vr)\, dr\right]^2 \tag{20}$$

The solution to this integral is (Ref. 14)

$$I(w,z_2) = (2\pi)^2 \, |K^2 \begin{bmatrix} \dfrac{z_1^{\,2}}{k_1 a} & \text{for } \dfrac{k_2 w}{z_2} < \dfrac{k_1 a}{z_1} \\[2ex] \dfrac{z_2}{2k_2 w} & \text{for } \dfrac{k_2 w}{z_2} = \dfrac{k_1 a}{z_1} \\[2ex] 0 & \text{for } \dfrac{k_2 w}{z_2} > \dfrac{k_1 a}{z_1} \end{bmatrix} \tag{21}$$

The edge of the particle image is defined by

$$w = \frac{k_1}{k_2}\,\frac{z_2}{z_1}\, a \tag{22}$$

and the particle is magnified by

$$m = \frac{k_1}{k_2}\,\frac{z_2}{z_1} \tag{23}$$

The image location, z_2, is found from the focusing condition and Eq. (19) and is

$$z_2 = \left(\frac{k_1}{k_2 z_1} - \frac{k_1}{k_2 R_1} - \frac{1}{R_2}\right)^{-1} \tag{24}$$

where $R_1 = a_1 + z_o$.

Thus, when the integral is over infinity and the focusing condition is applied, the magnified particle image reconstructs at z_2.

The special case of recording and reconstructing the hologram with plane waves can be found by multiplying the spherical wave intensity by z_o^4 and R_2^2 and taking the limit as z_o and R_2 go to infinity. The reason for multiplying by z_o^4 and R_2^2 is seen by noting that plane waves are described by $A_o \exp(ikz)$ while spherical waves are described by $\frac{A \exp(ikr)}{r}$. In the intensity equation these terms become A_o^2 and $\frac{A^2}{r^2}$, respectively, and the intensity equation must be multiplied by R_2^2 to remove these terms in the denominator. The term z_o is to the fourth power since the intensity is equal to the square of the integral containing the amplitude transmittance of the film, and the transmittance is proportional to the intensity recorded. The intensity resulting from plane waves is, therefore,

$$
\begin{aligned}
I_{p.w.}(w,z_2) &= \lim_{\substack{R_2 \to \infty \\ z_o \to \infty}} R_2^2 z_o^4 I_{s.w.}(w,z_2) \\
&= c^2 \left\{ \left[\int_o^H J_1(Dr) J_o(vr) \cos\left(\frac{u}{2} r^2\right) dr \right]^2 \right. \\
&\quad \left. - \left[\int_o^H J_1(Dr) J_o(vr) \sin\left(\frac{u}{2} r^2\right) dr \right]^2 \right\}
\end{aligned}
\tag{25}
$$

where

$$c = \frac{k_2^2 a}{2\pi z_2} \tag{26}$$

and

$$u = \frac{k_2}{z_2} - \frac{k_1}{z_1} \tag{27}$$

Although this is a particular condition of the more general spherical wave case, it has been found that data reduction of a volume of particles is more easily accomplished with plane waves because plane waves are easier to reproduce for the reconstruction and because the magnification will now always be unity for any k_2/k_1 ratio. The focusing condition implies that

$$z_2 = + \frac{k_2}{k_1} z_1 \tag{28}$$

The positive sign indicates, by convention, that the image is located to the right of the hologram plane.

The integral in Eq. (25) will be known as the focusing integral. Its solution for any and all w and z_2 can be done only by numerical integration. The computer program which was written to perform the integration is given in Appendix III. In order to simplify the limiting parameters of the hologram, the following special cases have been examined:

1. $k_1 = k_2 = k$ The same wavelength is used in recording and reconstruction.

2. $z_2 = z_1 + \eta$ The term η defines planes to the left and right of focus which occur when $z_2 = z_1$ (Fig. 1).

3. $H = \frac{\Omega \lambda z_1}{2\pi a}$ where Ω is the argument of the first-order Bessel Function $J_1\left(\frac{k_1 a H}{z_1}\right)$ at the upper limit, H, of the integral. Therefore, the limiting aperture of the hologram can be defined in terms of the number of zeros of $J_1(\Omega)$ recorded.

4. The F-number, F/#, of the hologram is $F/\# = \frac{z_1}{2H} = \frac{\pi a}{\lambda \Omega}$. (29)

   This parameter is important in that it allows the hologram imaging properties to be compared to a thin lens.

The integration method in the program is Gaussian. A 32- or 96-increment integration is available from an input command, the 96-increment Gaussian method being more accurate. The number of sine peaks, n, within the upper limit of the integral should, for the sake of accuracy, be less than the number of increments, where $n = \frac{N\Omega^2}{2\pi^2}$. Input data are the recording distance, z_1, wavelength, λ, far-field number, N, and Ω, the argument of $J_1(\Omega)$, which defines the upper limit of integration, H. Other input data are the minimum and maximum values of η/a (η normalized to the particle radius) and the increments of η/a, and the minimum and maximum values of w/a and its increments. Output data consist of z_1, λ, Ω, N, a, F/#, H, and I(0, 0) on the first data page. The term I(0, 0) is the intensity in the plane of focus at the center of the particle. It is the value to which the other intensities are normalized. The remaining data are $I_{norm}(\overline{w})$ tabulated for each w/a and η/a.

2.2 SPECIAL CASES OF THE FOCUSING INTEGRAL

In order to check the data from the computer program and also to analyze the output data and their trends, special cases of the focusing integral were evaluated. These cases for the most part were chosen because a closed form solution of the focusing integral could be derived.

2.2.1 Case 1 – Ideal Image of a Perfect Hologram

This case has already been studied for the spherical wave case, and the results will be repeated here for plane waves. In the focal plane, at u = 0 and H = ∞, the particle image intensity is

$$I(w,o) = c^2 \begin{bmatrix} \left(\frac{z_1}{k_1 a}\right)^2 & \text{for } w < a \\ \left(\frac{z_1}{2k_1 a}\right)^2 & \text{for } w = a \\ 0 & \text{for } w > a \end{bmatrix} \tag{30}$$

The ratio of the edge intensity to the central intensity is seen to be 1/4. At the edge of the particle, i.e., the point of discontinuity, the amplitude is found by taking the average of the upper and lower values (1/2). The intensity, therefore, is the square of this value, or 1/4 the intensity on the image center.

2.2.2 Case 2 – Intensity at the Image Center

All of the computer data are normalized to the intensity at the center of the particle image. For this case, where $\eta = w = 0$, the integral becomes

$$I(o,o) = \frac{c^2}{D^2}\left[\int_o^H J_1(Dr)\,dr\right]^2 = \frac{c^2}{D^2}\left[1 - J_o(\Omega)\right]^2 \tag{31}$$

Thus, as the limiting aperture varies, the central intensity of the particle image will oscillate.

2.2.3 Case 3 – Intensity at the Image Edge

For a finite aperture, the intensity at the edge of the particle image is .

$$I(a,o) = c^2 \left[\int_o^H J_o (Dr) J_1 (Dr) \, dr \right]^2 \tag{32}$$

where v = D for w = a.

From Gradshteyn and Ryzhik (Ref. 14), the solution to this integral is

$$I(a,o) = \frac{c^2}{D^2} \left[\sum_{n=o}^{\infty} J_{n+1}^2 (\omega) \right]^2 \tag{33}$$

Note that the intensity at the edge of the particle is a function of the limiting aperture only. As the aperture becomes large, it approaches the value given by Eq. (30) of Case 1 as a limit. The intensity variation I(a, o) normalized to this limit is shown in Fig. 2. The minima occur when $J_1 (\Omega)$ goes to zero, and the peaks occur when $J_o(\Omega)$ is zero. It has been shown (Ref. 15) that

$$2 \sum_{r=1}^{\infty} J_r^2 (\Omega) = 1 - J_o^2 (\Omega) \tag{34}$$

Thus, when Ω is a zero of $J_o(\Omega)$, the summation is a maximum. Differentiating with respect to Ω gives

$$\frac{d}{d\Omega} 2 \left[\sum_{r=1}^{\infty} J_r^2(\Omega) \right] = 2 J_o (\Omega) J_1 (\Omega) \tag{35}$$

Thus, the zeros of $J_1 (\Omega)$ are the minima of I. Figure 3 is the intensity, I(o, a), normalized to the intensity at the center of the particle, I(0, 0).

2.2.4 Case 4 – Gradient of Intensity at the Image Edge

The slope of the intensity at the edge of the in-focus particle can also be derived as a function of the limiting aperture. The intensity of the particle in focus is given by

$$I(w,o) = c'^2 \left[\int_o^H J_1 (Dr) J_o (vr) \, dr \right]^2 \tag{36}$$

Taking the derivative of I(w, o) with respect to w gives

$$\frac{d}{dw} I(o,w) = 2c^2 \left[\int_o^H J_o (vr) J_1 (Dr) dr \right] \left(- \frac{k}{z_1} \right) \int_o^H r J_1 (Dr) J_o (vr) dr \tag{37}$$

The integrals will be evaluated when w = a, therefore,

$$\frac{d}{dw} I(o,w)_{w=a} = -\left(\frac{2c^2 k}{z_1} \right) \int_o^H J_1 (Dr) J_o (Dr) dr \int_o^H J_1^2 (Dr) rdr \tag{38}$$

The second integral has a closed form solution (Ref. 15) given in general by

$$\int_o^\lambda z J_v^2 (kz) dz = \frac{1}{2} \lambda^2 J_v^2 (k\lambda) - J_{v-1} (k\lambda) J_{v+1} (k\lambda) \tag{39}$$

Therefore,

$$\int_o^H r J_1^2 (Dr) dr = \frac{H^2}{2} J_1^2 (HD) - J_o (HD) J_2 (HD)$$

Substituting this into Eq. (38) and recognizing the first integral as being the same as was solved in Case 3, Eq. (32), and that HD = Ω, then

$$\frac{d}{dw} I(o,w)_{w=a} = - \frac{k}{z_1} \frac{c^2 H^2}{D} \sum_{n=o}^{\infty} J_{n+1}^2 (\Omega) J_1^2 (\Omega) - J_o (\Omega) J_2 (\Omega)$$

$$= k^{12} \Omega^2 \sum_{n=o}^{\infty} J_{n+1}^2 (\Omega) J_1^2 (\Omega) - J_o (\Omega) J_2 (\Omega) \tag{40}$$

where

$$k^{12} = \frac{4aN^2}{\pi^2} c^2$$

The slope at the edge of the particle is seen to increase as the aperture radius squared. The graph of this equation is shown in Fig. 4. The "staircase" effect in Fig. 4 is a result of the Bessel functions. The increase in the slope is zero for Ω equal to a zero of the first-order Bessel function. Normalizing the slope to the intensity I(0, 0) produces the curve in Fig. 5. Here it is shown how the slope at w = a can actually be less for larger Ω values than for the smaller ones. The minima and maxima of the curve occur at zeros of J_1. This curve also approaches infinity as Ω approaches ∞. One other important point brought out in the normalization process is that the slope of this curve is inversely proportional to the radius, a. Thus, the edges of the smaller particles will be better defined for a given recorded Ω.

2.2.5 Case 5 – Intensity along the Image Axis

As a limiting case for the intensity away from the plane of focus, let $H \rightarrow \infty$ and $w = o$, i.e., the intensity as a function of η along the particle axis. This will be called the optic axis of the particle since the light distribution is symmetrical about this axis for each particle. This is evident from the fact that the intensity integral is independent of the polar angle ϕ. With these assumptions, the focusing integral becomes

$$I(n,o) = c^2 \left[\int_o^\infty \cos\left(\frac{u}{2} r^2\right) J_1 (Dr)\, dr \right]^2 + \left[\int_o^\infty \sin\left(\frac{u}{2} r^2\right) J_1 (Dr)\, dr \right]^2 \tag{41}$$

From Ref. 14 the closed form solutions of the sine and cosine integrals are

$$\int_o^\infty \sin\left(\frac{u}{2} r^2\right) J_1 (Dr)\, dr = \frac{1}{D} \sin\left(\frac{D^2}{2u}\right)$$

$$\int_o^\infty \cos\left(\frac{u}{2} r^2\right) J_1 (Dr)\, dr = \frac{2}{D} \sin^2\left(\frac{D^2}{4u}\right) \tag{42}$$

where $\frac{u}{2} > 0$ and $D > 0$. Substituting these solutions into the equation gives

$$I(n,o) = c^2 \frac{1}{D^2} \sin^2\left(\frac{D^2}{2u}\right) + \frac{4}{D^2} \sin^4\left(\frac{D^2}{4u}\right) \tag{43}$$

Using the trigometric identity

$$2 \sin^2 \frac{x}{2} = 1 - \cos x$$

the intensity along the optic axis of the particle becomes

$$I(n,o) = \frac{4c^2}{D^2} \sin^2 \left[\frac{\pi}{8N} \left(\frac{z_1}{n} + 1\right)\right] \tag{44}$$

where D and u have been replaced by their definitions and $\eta > 0$. This is a sinusoidally varying function which increases in frequency as η approaches 0. The frequency ν as a function of η is

$$\nu = - \frac{\pi}{8N} \frac{z_1}{\eta^2} \tag{45}$$

The last minima and maxima from the focal plane occur when

$$\eta_{max} = \frac{z_1}{4N - 1} \approx \frac{z_1}{4N}$$

$$\eta_{min} = \frac{z_1}{8N - 1} \approx \frac{z_1}{8N} \tag{46}$$

Figure 6 illustrates the variation of I along the axis for N = 1, 10, 100. The intensity is normalized to the intensity at I(0, 0) which is simply a constant, C^2/D^2, for $\Omega = \infty$. The horizontal axis is in terms of η/a^2 to allow the curve to be drawn for all particle radii and recording distances. As the particle image is brought into focus, the intensity along the axis oscillates rapidly with z.

Cases 2, 3, and 4 apply equally well to spherical wave analysis since the argument $J_1(\Omega)$ is the same for plane and spherical waves. The edge of the image would now correspond to w = ma, where the constant in front of the solutions to the integrals will be the only difference. For Case 5, u is replaced by u′ for spherical waves, and, therefore, the frequency of oscillation and the points of minima and maxima will be functions of the positions of the sources s and s′, and the particle position.

2.3 DATA FROM THE FOCUSING INTEGRAL

The intensity distribution about the plane of focus is a function of a number of parameters (e.g., particle size, recording distance, and limiting aperture). Therefore, in order to obtain curves from the computer data which have meaning for the largest number of cases, the parameters u and v in the intensity integral were chosen for the horizontal and vertical axes, where

$$u = \frac{\lambda}{2\pi} \frac{\Omega^2}{a^2} \eta \frac{z_1}{z_1 + \eta}$$

$$v = \frac{\Omega}{a} w \frac{z_1}{z_1 + \eta} \tag{47}$$

As is evident from these equations, u and v are not independent for $\eta = f(z_1)$. They are linearly related as

$$v = (\Omega - \frac{1}{2N\Omega} u) m \tag{48}$$

where m = w/a. The intensity along any line parallel to the optic axis can, therefore, be constructed on a graph and the intensity variation observed as η varies. Isophote diagrams (i.e., lines of constant intensity) are used to display the computer data. For a constant Ω, each

isophote diagram represents the conditions for any particle radius, a, and recording distance, z_1, as well as wavelength. Only positive v is shown in all the diagrams except for one, since the intensity variation for v is symmetric about the optic axis. The diagram is also symmetric about the v axis since $|a + ib|^2 = |a - ib|^2$.

Some typical isophote diagrams are shown in Figs. 7 through 11. Dashed lines on the diagrams indicate the intensity variation along a line adjacent to the particle edge and parallel to the optic axis as illustrated in Fig. 7. This line is found by letting m = 1 in Eq. (48). For small Ω, as in Fig. 7, where $\Omega = 3.832$, i.e., the first zero of $J_0(\Omega)$ (the Airy Disk), the intensity variation at w = a is seen to be extremely unsymmetrical as predicted by Eq. (4). More will be said about this later when in-focus criteria for the image will be defined.

Figure 8 is the isophote diagram for $\Omega = 5.0$. The intensity variations are shown to be more complex about the focal plane. Figures 9 and 11 correspond to the second and fourth zeros of $J_1(\Omega)$, respectively. Figure 10 illustrates the complexity of intensity variations as Ω becomes larger. Here $\Omega = 11.5$. To illustrate the 360-deg intensity variations, all four quadrants of the u and v space are shown.

To better illustrate the variations of intensity for various particle radii and recording distance, graphs of $I(w, \eta)$ versus w/a and η/a are presented. The coordinates w/a and η/a are used to indicate the distance in particle radii from its center. Figures 12 to 16 illustrate the intensity variations for typical particle radii and recording distances in selected planes out of focus. These would be the intensity variations one would observe over the image of the particle as planes of focus were observed.

Figures 17 to 21 show the intensity variations along η for the optic axis and the edge of the particle as the image is brought in and out of focus. These curves will be used to define the criterion for particle size resolution and the focal tolerance (depth-of-field) of the hologram.

2.4 VALIDITY OF SCALAR DIFFRACTION THEORY

The expressions derived so far are all based on a scalar diffraction theory, which is not valid in general. Under certain conditions the vector nature of the electromagnetic wave must be taken into account. This occurs, for example, at small F/# ratios. It also occurs under some polarization conditions. Finally scalar diffraction is not applicable in

the proximity of a boundary. The complexity of the more general vector diffraction theory encourages the use of the scalar approximation, which should be acceptable for most of the cases covered here.

SECTION III
THEORETICAL RESOLUTION

An accurate determination of size and position of the reconstructed image is important for measuring the velocity and size distribution of particles in a volume. From the foregoing data a number of techniques may be postulated by which to determine the ultimate accuracy of such an instrument. The limits of resolution which will be formulated will be entirely theoretical. It must be remembered, therefore, that, in practice, the experimental data can be worse than this. These will give an indication of the theoretically achievable resolution.

3.1 PARTICLE POSITION

The smallest particle that can be resolved by the in-line hologram is

$$a_{min} = -\frac{0.61\lambda z_1}{H} \tag{49}$$

where it was assumed that the first zero of the first-order Bessel function is recorded. The data from the isophote diagram for $\Omega = 3.832$ corresponds to this minimum resolvable radius.

The in-focus particle image will not, in general, be the same size as the particle itself even with plane wave recording and reconstructing beams. This is because the edge of the particle image has a finite slope and, as shown in Figs. 4 and 5 and Figs. 12 to 16, the intensity at the edge of the particle is not the same for different limiting apertures, Ω. Each particle will have a different Ω associated with it according to its size and distance from the hologram. Thus, a criterion must be chosen which will enable an instrument to measure the particle size. The criterion which will be used is the intensity limit at the particle edge given by Eq. (30), i.e., $I_{norm} = 0.25$ where $\eta = \infty$. Figure 3 shows that the intensity oscillates about this value and approaches it as the radius of the limiting aperture increases. The edge will be assumed to lie at the point where the intensity is 25 percent of that at the center. The accuracy of the measurement, therefore, will depend, theoretically, on how much

of the Bessel function can be recorded, and the maximum error will be a function of Ω. Taking the derivative of $I_{norm}(a, o)$ with respect to Ω shows that the extremes occur at the zeros of $J_1(\Omega)$. From the isophote diagrams, Figs. 7 to 11, the distance Δv, corresponding to the change in intensity at the known edge to where it is 25 percent of the center intensity, was found. Using Eq. (47) this value can be expressed as a percent of particle radius, as

$$\Delta m = \Delta \left(\frac{v}{\pi}\right) \frac{\pi}{\Omega} \times 100 \text{ percent} \tag{50}$$

It is shown that the error is the same for all particle radii at a given constant recorded Ω. Table I, Appendix II, lists the percent error for typical Ω. The errors designated as maximum correspond to the Ω at the extreme of the curve in Fig. 3.

All limiting apertures above $\Omega = 7.016$ have images which contain peaks making possible a second criterion for the maximum possible theoretical error of the images. These maxima occur just before the edge and exceed the intensity at the center of the particle image. This is shown in Figs. 12 to 16. These peaks can be detected and the particle size can be found to within this accuracy. The errors arising from this measurement are given in Table II. These values were taken from the isophote diagrams for the respective values of Ω. Note, however, that for $\Omega = 5$ and 3.832 there are no peaks involved. Thus, the error involved in these cases is entirely a function of the ability of the detector to measure the 25-percent point. On film, if the exposure level of the recorded image is small, only the relatively large central peak of the intensity will be recorded.

The particle position is important since it completes the data for the particle size distribution in the volume and when the recording is taken with a double pulse, it gives the velocity of the particle. The position of the particle in the plane of focus (i.e., the p, q, plane of Fig. 1b) is accurate to the limits set by the Rayleigh criterion, i.e., when the principal intensity maxima of one particle lies at the first minimum of the other the particles are just resolved. For plane waves, therefore, the particle separation, S_p, is (Ref. 4)

$$s_p = - \frac{0.61\lambda z}{a} = 2.44 \text{ Na} \tag{51}$$

However, the plane of focus of the particle (occurring when $\eta = 0$) is less accurately known than this. The accuracy limits set by the hologram will, therefore, define the focal tolerance, $\Delta\eta$, of the hologram.

To find the $\Delta\eta$ resolution of the reconstructed image, the isophote diagrams and Figs. 17 to 21 will be used. From these data a number of methods of measuring the focal tolerance (depth of field) of the in-line hologram are evident. The first consists of measuring the intensity change on the image as it is brought into and out of focus.

The point that would be observed could be at the particle center, its edge, or even a slight distance away from the edge. Another method would be to measure the slope at the edge of the particle and determine when it becomes maximum. Measuring the slope change would entail an instrument continuously scanning the particle as it is moved out of focus and a logic network to compare one slope measurement to the preceding one. Conceivably this can be done with a television camera and some logic circuitry.

At the center of the particle image the criterion that a change in intensity of 20 percent can be detected will be used. From the definition of the horizontal axis, u, of the isophote diagrams, the change in η is

$$\Delta\eta = \pm \frac{2\pi^2}{\lambda} \frac{a^2}{\Omega^2} \Delta\left(\frac{u}{\pi}\right) \tag{52}$$

The value of $\Delta\left(\frac{u}{\pi}\right)$ can be taken from the isophote diagrams. The focal tolerance, $\Delta\eta$, therefore, will apply for all particle diffraction patterns having the same upper limit of the Bessel function. Equation (52) can be rewritten as

$$\Delta\eta = \pm k_{holo}(\Omega) \frac{a^2}{\lambda} \tag{53}$$

where

$$k_{holo}(\Omega) = \frac{2\pi^2}{\Omega^2} \Delta\left(\frac{u}{\pi}\right)$$

The values of $K_{holo}(\Omega)$ for each Ω are given in Table III along with the corresponding $\Delta\left(\frac{u}{\pi}\right)$ from the isophote diagrams. Notice that the accuracy improves as Ω increases. For $\Omega = 7.016$ and $\lambda = 6328$ Å, the focal tolerance of a hologram of a 50-μm particle is ± 635 μm. However, for a 10-μm particle the focal tolerance reduces to ± 25.4 μm. All $\Delta\left(\frac{u}{\pi}\right)$, except when $\Omega = 3.832$, were measured at a 20-percent increase in the intensity.

An ideal thin lens imaging a point source has a focal tolerance given by (Ref. 13)

$$\Delta\eta = \pm 3.2 \frac{\lambda}{\pi} (F/\#)^2 \tag{54}$$

where F/# is the F number of the lens. To compare this to the hologram, the F/# of the thin lens will be assumed to be the same as that of the hologram. Substituting the definition of the F/# for the hologram (Eq. (29)) into this equation gives

$$\Delta\eta = \pm \frac{20.1}{\Omega^2} \frac{a^2}{\lambda} = k_{T.L.}(\Omega) \frac{a^2}{\lambda} \tag{55}$$

The thin-lens focal tolerance is of the same form as that obtained from the hologram since the same coordinate relationship to η was used in both cases. The value of $K_{T.L.}(\Omega)$ for the thin lens is given in Table III. It is shown that the criterion chosen for the hologram yields results for the $\Delta\eta$ position of the particle which are comparable to a thin lens.

The intensity change at the center of the image was shown in Section 2.2.5, where $\Omega = \infty$ is an oscillating function of η. For this limiting case, a detector would not need to recognize an intensity change of a given amount. Rather, the spatial frequency of the intensity could be observed until the cutoff frequency of the detector or its associated electronics was reached. This method could conceivably further increase the resolution. For the small limiting apertures, the errors associated with measuring the position of this extrema at the center of the particle are large. The values of $K_{holo}(\Omega)$ for this criterion are also given in Table III.

Observing the intensity change at the edge of the particle has its inherent difficulties, the first of which is finding the true particle edge. As was shown previously, this value can have a theoretical error of as much as 20.5 percent. Also, as indicated by the dashed lines signifying a line tangent to the edge of the particle and parallel to the optic axis, the intensity is not symmetric on either side of focus, except for large Ω and N. A worse-case condition was shown in Fig. 12 where $\Omega = 3.832$ and N = 5. The intensity past the point of focus is much greater than at the focal point. This phenomenon is observed upon reconstruction as an intensity increase in the particle image past the focal plane. If a minimum detectable intensity change of 20 percent of that in the plane of focus is used, then Fig. 11, where $\Omega = 13.324$, indicates that this value will not be reached until $u > 9\pi$ which is at least nine times poorer than the resolution associated with measuring the center intensity.

The third point under consideration as an indication of the Δz resolution is at $w = a^+$ where a^+ is some distance beyond the edge of the image. When the image is observed with the eye, out-of-focus planes are seen as containing an enlarged image with fuzzy edges. This corresponds to the intensity beyond the particle edge increasing. Here, as in the case of observing the edge of the particle, difficulties arise in finding the edge without a prior knowledge of the particle size.

Criteria for the particle size and position have been defined in terms of an intensity change. The theoretical resolution of the particle size is seen to be better than 20.5 percent for a worse-case condition, i.e., only the first zero of the first Bessel function is recorded. Equation (50) shows that this resolution is only a function of the limiting aperture, Ω. On the other hand, the depth of field of the hologram is approximately the same as a thin lens. Equation (52) shows that the focal tolerance, $\Delta\eta$, is a function of the limiting aperture and the particle radius. This can be related back to the F/# of the hologram to give

$$\Delta\eta = \pm\ 2\lambda\ (F/\#)^2\ \Delta\left(\frac{u}{\pi}\right) \tag{56}$$

The smaller the F/# is the better will be the focal tolerance and, therefore, z_1 and the separation between two image planes can be more accurately found.

3.2 LIMITING PARAMETERS OF THE FILM

Up to this point nothing has been said about the causes of the limiting aperture other than the fact that there is one and that it keeps the reconstructed image plane and the image from being exactly known. The film can limit the aperture of the recorded diffraction pattern in two ways. First, because of the linearly increasing frequency of the sine term in the recorded intensity at some point on the film, (Eq. (2)) the frequency will exceed that which can be recorded. Secondly, inherent on the film is its grain structure which introduces noise into the recorded signal. The decreasing peak amplitude of the Bessel function in the interference term in Eq. (2) and the $1/r$ dependence of the intensity causes a reduction in signal amplitude as r increases. At some point on the film, r_{max}, the signal will be engulfed in noise and will be ineffective.

The cutoff frequency of the film is related to the recording parameters through the sine term. The derivative of its argument with respect to r is the frequency, ν, at a given r, i.e. (assuming an M.T.F. of unity),

$$\nu = \frac{r}{\lambda z_1} \tag{57}$$

The radius, r_{max}, corresponding to the maximum cutoff frequency of the film is, therefore,

$$r_{max} = \nu_{max}\lambda z_1 = 4Na^2\nu_{max} \tag{58}$$

where $z = \frac{N4a^2}{\lambda}$ was used. This is the radius of the limiting aperture set by the film cutoff frequency. The maximum argument, Ω_{max}, of the first-order Bessel function is

$$\Omega_{max} = 2\pi a\, \nu_{max} \tag{59}$$

As an example, assume Kodak® SO-243 film is used as the recording medium; it has a cutoff frequency of about 200 lines/mm. For a 50-μm particle, therefore, the film will record the Bessel function until its argument is 20π. The size of this aperture is 2N mm, N being the number of far fields the film is from the particle. Table IV shows r_{max} and Ω_{max} for a range of particle sizes. The values of r_{max} below the heavy line will not be limited by the cutoff frequency of a 4- by 5-in. sheet of film, but rather its size.

The minimum F/# the film may have is found from Eq. (29) and Eq. (59) and is given by

$$F/\#_{max} = \frac{1}{2\lambda\nu_{max}} \tag{60}$$

The F/# is seen to be as good as the film cutoff frequency. For SO-243 film and λ = 6328 Å the smallest F/# attainable by this film is 3.95.

The Δz resolution was shown previously to be (Eq. (52))

$$\Delta\eta = \pm \frac{2\pi^2}{\lambda} \frac{a^2}{r^2} \Delta\left(\frac{u}{\pi}\right)$$

Substituting Eq. (59) for Ω gives

$$\Delta\eta/\text{min} = \pm \frac{1}{2\pi\lambda} \frac{1}{\nu^2_{max}} \Delta\left(\frac{u}{\pi}\right) \tag{61}$$

The resolution of the particle position is seen to depend on the maximum recordable frequency. For SO-243, $\Delta\eta = \pm 6.3 \times 10^{-6}\, \Delta\left(\frac{u}{\pi}\right)$. Thus, this relatively low resolution film is capable of resolving the focal plane to better than ±10 μm, assuming, that is, that the cutoff frequency is the major limiting parameter.

From Eq. (49) it is seen that the minimum resolvable particle radius can also be expressed in terms of the cutoff frequency as

$$a_{min} = \frac{0.61}{\nu_{max}} \tag{62}$$

From this equation, SO-243 is capable of resolving particle radii as small as 3.15 μm.

The resolution capabilities of the hologram for small particles appear from the foregoing criteria specifications to be extremely good for a relatively low frequency film. However, as stated before, the cutoff frequency is not the only limiting parameter of the film. The film grain noise which is present on the recorded signal is also a limiting factor.

The film noise is measured in rms granularity and is defined as (Ref. 16)

$$\sigma(D) \equiv \sqrt{\frac{\Sigma \Delta D_i^2}{n-1}} \tag{63}$$

where ΔD_i is the deviation of n density readings. In practice the rms granularity is measured by scanning an aperture of area A over the film. The granularity is given to a good approximation as (Ref. 16)

$$\sigma(D) = \frac{G\sqrt{\bar{D}}}{\sqrt{A}} \tag{64}$$

where $\bar{D}$ is the average density on the film and G, which is the Selwyn granularity, is $G = 2\sqrt{0.43\pi}\,\bar{d}$, where $\bar{d}$ is the mean diameter of a developed grain. The granularity is seen to have a reciprocal relationship to the scanning aperture.

The signal-to-noise ratio (SNR) of the film is

$$SNR = \frac{\bar{D}_B - \bar{D}_S}{\sigma(D)} \tag{65}$$

where $\bar{D}_B$ is the average density of the background and $\bar{D}_S$ is the average density of the signal. The normalized intensity incident on the film is given by

$$I_{norm} = 1 - \frac{\pi}{N} \frac{J_1(\Omega)}{\Omega} \sin\left(\frac{\pi r^2}{\lambda z_1}\right) \tag{66}$$

where plane wave recording is assumed and the third term has been dropped since it is negligible. Since $\frac{\pi}{N}\frac{J_1(\Omega)}{\Omega}$ modulates the sine term, the peak magnitude of this term will only be considered. The signal density recorded by the film is (Ref. 17)

$$D = \gamma \operatorname{Log}_{10}(It) + D_o \tag{67}$$

where γ is the slope of the characteristic curve for the film, t is the exposure time and D_o is the density where the linear portion of the curve intersects the vertical axis. Grouping the constants together gives

$$D = \gamma \operatorname{Log}_{10} I + K \tag{68}$$

where

$$K = \gamma \operatorname{Log}_{10} t + D_o$$

The intensity, I, can be decomposed into a signal I_S and background, I_B, and D becomes

$$D = \gamma \operatorname{Log}_{10}\left(1 + \frac{I_S}{I_B}\right) + K' \tag{69}$$

Here $K' = K + \gamma \operatorname{Log}_{10} I_B$ and the signal intensity has been normalized to the background. Since $I_B > I_S$ the logarithm can be expanded as

$$\operatorname{Log}_{10}(1 + x) = \frac{1}{2.303}\left[x - \tfrac{1}{2}x^2 + \ldots\right] \approx \frac{1}{2.303}x$$

Therefore, the density on the film resulting from the plane waves and diffracted light off the particle is

$$D = -\frac{\gamma\pi}{2.303N}\frac{J_1(\Omega)}{\Omega} + K' \tag{70}$$

K' represents the average background density $\overline{D}_B$. Therefore, Eq. (65) becomes

$$\mathrm{SNR} = \frac{\gamma\pi}{2.303N}\frac{J_1(\Omega)}{\Omega}\frac{1}{\sigma(D)} \tag{71}$$

$$= \frac{\gamma\pi}{2.303NG}\frac{\sqrt{A}}{\sqrt{D}}\frac{J_1(\Omega)}{\Omega} \tag{72}$$

where Eq. (64) was used.

It is shown that as the area of the scanning aperture increases or equivalently when the area of the recorded signal density is large the SNR is maximized.

A half period of the sine function can be assumed to be recorded on the film as an annular region since the diffraction is symmetrical about the optic axis of the particle, i.e., its center. This is illustrated in Fig. 22. The area of this region is

$$A = \pi (r_2^2 - r_1^2) \tag{73}$$

where r_1 and r_2 are the radii of the inner and outer regions, respectively. The terms r_1 and r_2 correspond to consecutive zeros of the sine term. Since $r_2 = r_1 + \Delta r$, Δr can be found from this term and is

$$\Delta r = \frac{\pi z_1}{k r_1} \tag{74}$$

where it is assumed that $\Delta r < r_1$. The area of the annulus is now

$$A = \pi \lambda z_1 \tag{75}$$

This is seen to be independent of r for a constant z_1, just as the half-period zones of a Fresnel lens (Ref. 18). Using this area and $z_1 = \frac{N4a^2}{\lambda}$, Eq. (72) becomes

$$\mathrm{SNR} = \frac{2\gamma\pi\sqrt{\pi}}{2.303\, G\sqrt{\overline{D}_{rec}}} \quad \frac{a}{\sqrt{N}} \quad \frac{J_1(\Omega)}{\Omega} \tag{76}$$

In terms of the rms granularity of the film, the average density at which it was measured, $\overline{D}_{scan}$, and the diameter of the scanning aperture, d_{aper}, the SNR becomes

$$\mathrm{SNR} = \frac{4\gamma\pi}{2.303\sigma\,(D) d_{aper}} \quad \frac{\sqrt{D_{scan}}}{\sqrt{D_{rec}}} \quad \frac{a}{\sqrt{N}} \quad \frac{J_1(\Omega)}{\Omega} \tag{77}$$

This equation and Eqs. (71) and (72) represent the SNR of the film for the diffraction pattern recorded on an average background density $\overline{D}_{rec}$ and with a film gamma of γ. The quantity $J_1(\Omega)/\Omega$ is shown as a function of Ω in Fig. 23. The peak amplitudes of the first-order Bessel function were used for this figure. It is assumed that the signal is completely lost in the noise when the peak of $J_1(\Omega)$ is below the noise level.

For a given SNR and granularity the limiting aperture radius can be found. Table V gives the maximum Bessel function argument, Ω_{max},

recorded and the limiting aperture size of the diffraction patterns for typical particles and far-field numbers with SNR = 1. These are assumed to be recorded on SO-243 film which has an rms granularity of 7.4×10^{-3} measured with a 48-μm-diam aperture and a mean density of 1 (Ref. 19). It has been assumed that $\overline{D}_{rec} = \overline{D}_{scan}$ and $\gamma = 2.2$. The larger particles are shown to be limited not by the film grain noise but by either the film size or the size of the beam illuminating the particle field. Maximum radii below the dashed line in the table are larger than a 4- by 5-in. sheet of film.

Comparing Tables IV and V, it is seen that the size of the hologram on the film can be limited by either the film cutoff frequency or noise depending upon the far-field number and the particle size. In Table V all values of Ω_{max} below the solid line are smaller than the maximum Ω of the cutoff frequency for that particle radius. Thus, above this line the hologram size is limited by the cutoff frequency.

Besides the effects of the film grain and cutoff frequency, system noise is also responsible for limiting the hologram size. This noise can include dust and dirt in the system, an inhomogeneous wavefront illuminating the particle volume, and improper film developing techniques. These for the most part, however, are not predictable.

SECTION IV
SUMMARY AND CONCLUSIONS

From the intensity distribution recorded in an in-line hologram, the integral describing the intensity distribution about the reconstructed real image was found. Because of its complexity, only after special conditions were imposed upon this integral could it be solved in closed form. In general, numerical integration was necessary for its solution. The data from the integration was put in the form of isophote diagrams with hybrid u-v coordinates corresponding to constants within the arguments of the functions integrated. These diagrams which illustrate the lines of constant intensity about the particle image apply to all cases of particle radii and recording distances. The limiting aperture of the hologram, Ω, or more correctly, the upper limit of the argument of the first-order Bessel function, was the parameter which was different in each of the diagrams.

Resolution of the in-line hologram was found from the isophote diagrams by specifying certain criteria which define the particle image edge and its in-focus limits. Because of the finite slope of the reconstructed image edge, two criteria were presented for consideration.

The first took advantage of the fact that the squared average of the light amplitude at the edge of an image formed with all the light diffracted from the particle was 25 percent of the particle intensity. The inherent error in choosing this point was seen to be maximum when the aperture cutoff was at a zero of the first-order Bessel function. (The error was zero when the cutoff was a zero of the zeroth-order Bessel function.) Recording only the essential Airy Disk of $J_1(\Omega)$, i.e., its first zero, yields an error of 20.5 percent, the largest possible theoretically. As Ω increases this maximum error reduces to zero. The second criterion was formulated on the observation that the particle image contained peaks in intensity preceding the edge. If the last peak before the edge could only be discerned from the background, the error in the particle radius measurement would then be 45 percent for $\Omega = 7.016$ and 20 percent for $\Omega = 13.324$. As Ω increases the accuracy also gets better. This criterion could not be used for $\Omega = 3.832$ and $\Omega = 5$ since their images contained only a central peak.

The planar resolution containing the in-focus image ideally should be infinitesimally small. This would allow the image to be located at a precise distance, z_1, from the hologram and the distance between two images, Δz, could accurately be found for velocity data. However, because of the limited hologram size, the image contains in-focus characteristics over a finite distance, $\Delta\eta$. Minimum changes in these characteristics, therefore, can be used to define the focal tolerance or depth-of-field of the image. As the image is moved through focus, the data showed that the intensity and the slope at the edge of the image change. The center of the image, the particle edge, and a point away from the edge could be observed as to their intensity variations. Because of the error inherent in locating the edge and determining a fixed point away from it for all particles and recording distances, the intensity at these points and the slope change were not considered.

At the center of the image the criterion that a minimum intensity change of 20 percent could be detected was chosen. The data from the isophote diagrams showed that with this criterion the hologram has the same focal tolerance, $\Delta\eta$, as a thin lens, and $\Delta\eta$ is a function of the F/# of the hologram. In terms of the particle radius

$$\Delta\eta = \pm K_{Holo}(\Omega) \frac{a^2}{\lambda}$$

where $K(\Omega)$ is a constant for each maximum $J_1(\Omega)$ argument, and its value is given in Table III. For example, the focal plane of a 20-μm particle image can be found to within 100 μm if only the second zero of $J_1(\Omega)$ is recorded.

The intensity at the center of the image was found to oscillate as it is moved out of focus. If the last peak before the focal plane is used as the in-focus criterion, the focal tolerance is approximately double that found by the 20 percent intensity change criterion. $K_{hologram\ first\ extrema}(\Omega)$ in Table III is seen in most cases to be twice $K_{holo}(\Omega)_{20\%I}$.

The limited effective size of the hologram was shown to be the factor reducing the accuracy of the measurements of the reconstructed image size and z location. The parameters which cause this limiting aperture effect on the film are the cutoff frequency of the film, its grain noise, system noise (such as unwanted diffraction patterns from dust and other particles), film size, and reference beam size. Diffraction patterns of small particles ($<50\mu m$) recorded in small far-field distances were found to be limited for Kodak SO-243 by the cutoff frequency. The medium range particles ($50\mu m < a < 100\mu m$) diffraction patterns are limited by the loss of signal in the grain noise, and the larger particle ($a > 100\mu m$) patterns are limited by either the film size or the reference beam size. System noise will reduce these limits even more.

The focal tolerance, $\Delta\eta$, and the minimum resolvable particle radius, a_{min}, were expressed in terms of the cutoff frequency. This parameter could be used as a rule-of-thumb indicator for film quality since both of the limiting parameters of the film are related to a common source, the film grain. Kodak SO-243 film with a conservative cutoff frequency of 200 lines/mm is capable of resolving a 3-μm particle to within $\pm 10\ \mu m$.

Future work will include experimental verification of the theoretical results obtained here. Low, medium, and high granularity film will be used. The results obtained for the SNR will be compared to the reconstructed image and the measured film noise. The intensity changes about the particle image will be verified. Criteria for clean reconstructed images will be established to check the correctness of the theoretical criteria chosen.

Theoretically, future work can continue in improving the measurement of image separation by studying interference effects between two images separated by a distance less than their diameters. The theory can also be extended to spherical waves and the hologram resolution as a function of the total magnification. This could be compared to that obtainable from thin-lens magnification so that an engineering criterion can be evolved to pick between them.

REFERENCES

1. Thompson, B. J., Ward, J. H., and Zinky, W. R. "Application of Hologram Techniques for Particle Size Analysis." Applied Optics, 6:519-526, March, 1967.

2. Zinky, W. R. "Hologram Camera and Reconstruction System for Assessment of Explosively Generated Aerosols." U. S. Army Edgewood Arsenal TO-B-65-90, Chemical Research and Development Laboratories, Edgewood Arsenal, Maryland, October, 1965.

3. Trolinger, J. D., Belz, R. A., and Farmer, W. M. "Holographic Techniques for the Study of Dynamic Particle Fields." Applied Optics, 8:957-961, May, 1969.

4. Stroke, G. W. An Introduction to Coherent Optics and Holography. Academic Press, New York, 1969.

5. Trolinger, J. D., Belz, R. A., and Farmer, W. M. "Applications of Holography in Environmental Science." Paper presented at the 15th Annual Technical Meeting of the Institute of Environmental Sciences, Anaheim, California, April, 1969.

6. Fourney, M. E., Matkin, J. H., and Waggoner, A. P. "Aerosol Size and Velocity Determination Via Holography." The Review of Scientific Instruments, 40:205-213, February, 1969.

7. Shofner, F. M. et al. "Fundamentals of Holographic Velocimetry." Proceedings, 1969 International Congress on Instrumentation in Aerospace Simulation Facilities, May, 1969.

8. Farmer, W. M. Dynamic Holography of Small Particle Fields Using a Q-Spoiled Laser." Master's thesis, The University of Tennessee, Knoxville, 1968.

9. Thompson, B. J. "A New Method of Measuring Particle Size by Diffraction Techniques." Japanese Journal of Applied Physics, 4:302-307, Supplement I, 1965.

10. Belz, R. A. "Analysis of the Techniques for Measuring Particle Size and Distribution from Fraunhofer Diffraction Patterns." AEDC-TR-68-125 (AD674741), September 1968.

11. Shofner, F. M. et al. "Processing Holographic Velocimetry Data." Proceedings, 1969 International Congress on Instrumentation in Aerospace Simulation Facilities, May, 1969.

12. Develis, J. B., and Reynolds, G. O. Theory and Applications of Holography. Addison-Wesley Publishing Company, Reading, Massachusetts, 1967.

13. Born, M., and Wolf, E. Principles of Optics. Pergamon Press, New York, 1965.

14. Gradshtyn, I. S., and Ryzhik, I. M. Table of Integrals, Series, and Products. Academic Press, New York, 1965.

15. Watson, G. N. A Treatise on the Theory of Bessel Functions. Cambridge University Press, New York, 1952.

16. Higgins, G. C. "Methods for Engineering Photographic Systems." Applied Optics, 3:1-10, January, 1964.

17. Goodman, J. W. Introduction to Fourier Optics. McGraw-Hill Book Company, Inc., New York, 1968.

18. Jenkins, F. A., and White, H. E. Fundamentals of Optics. McGraw-Hill Book Company, Inc., New York, 1957.

19. Kodak Plates and Film for Science and Industry, Kodak Publication No. P-9, Rochester, New York, Eastman Kodak Company, 1967.

APPENDIXES

I. ILLUSTRATIONS
II. TABLES
III. COMPUTER PROGRAM FOR THE FOCUSING INTEGRAL

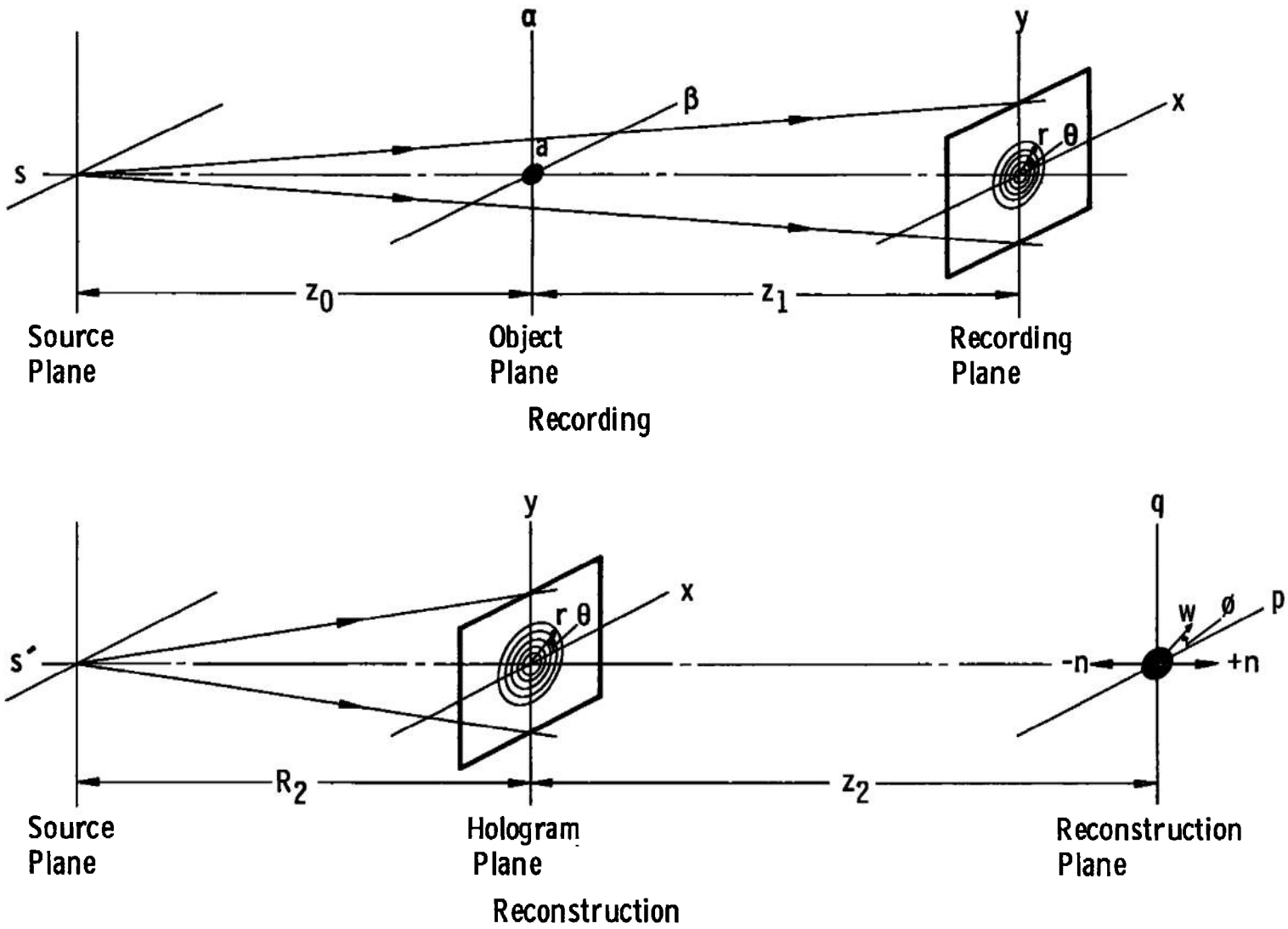

Fig. 1 Hologram Recording and Reconstruction with Spherical Waves

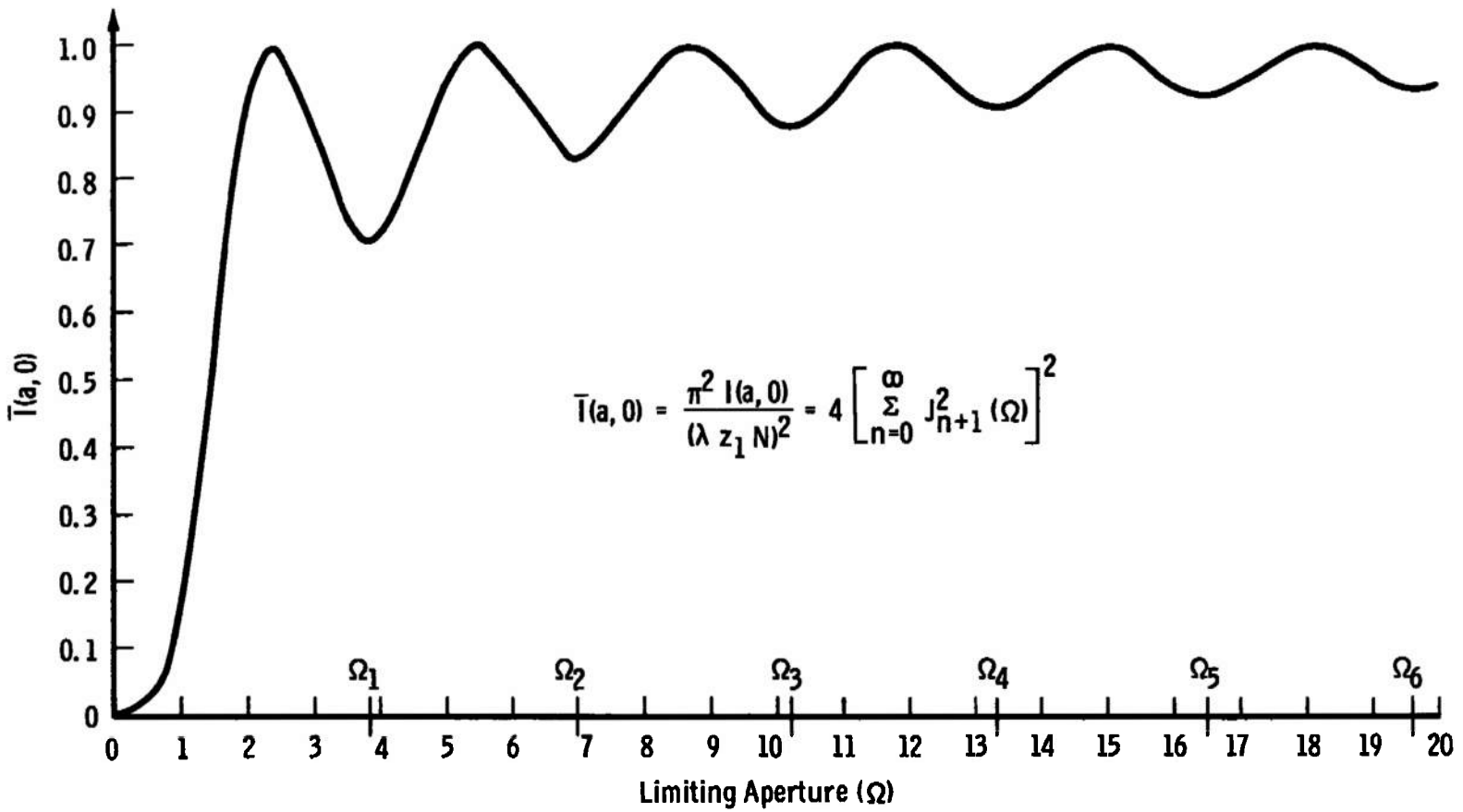

Fig. 2 Intensity at the Edge of the Particle Image

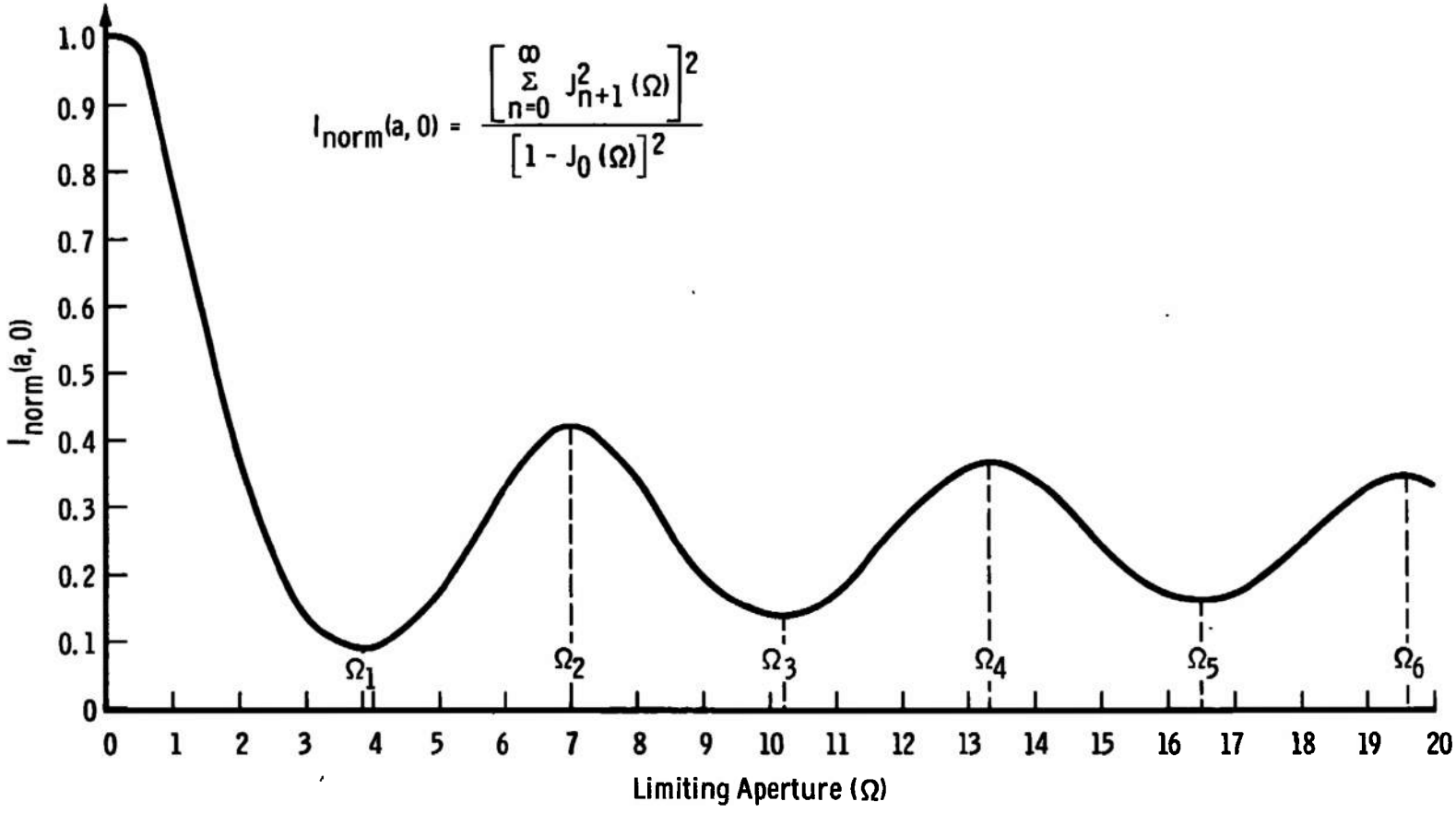

Fig. 3 Normalized Intensity at the Edge of the Particle Image

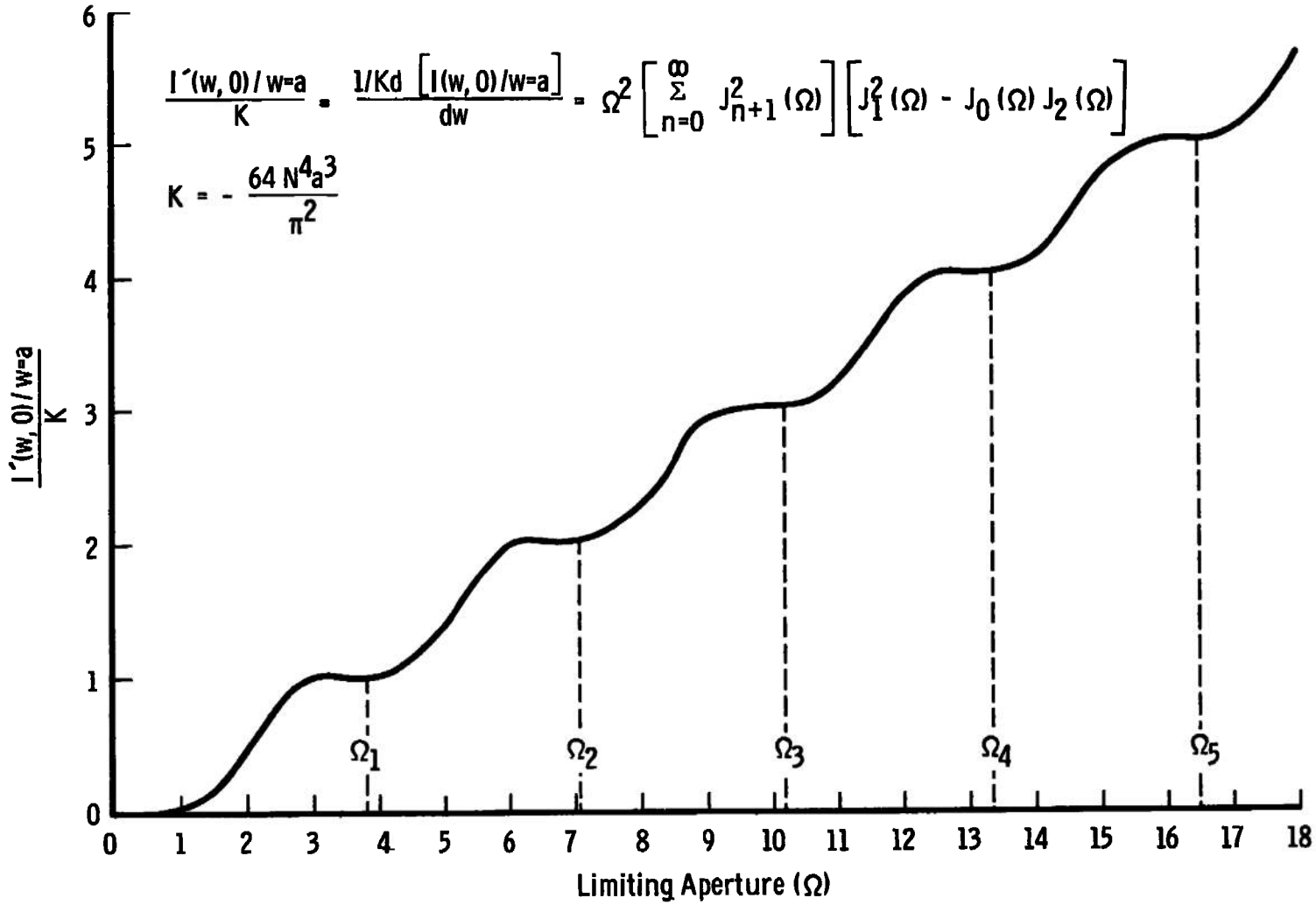

Fig. 4 Slope at the Edge of the Particle Image

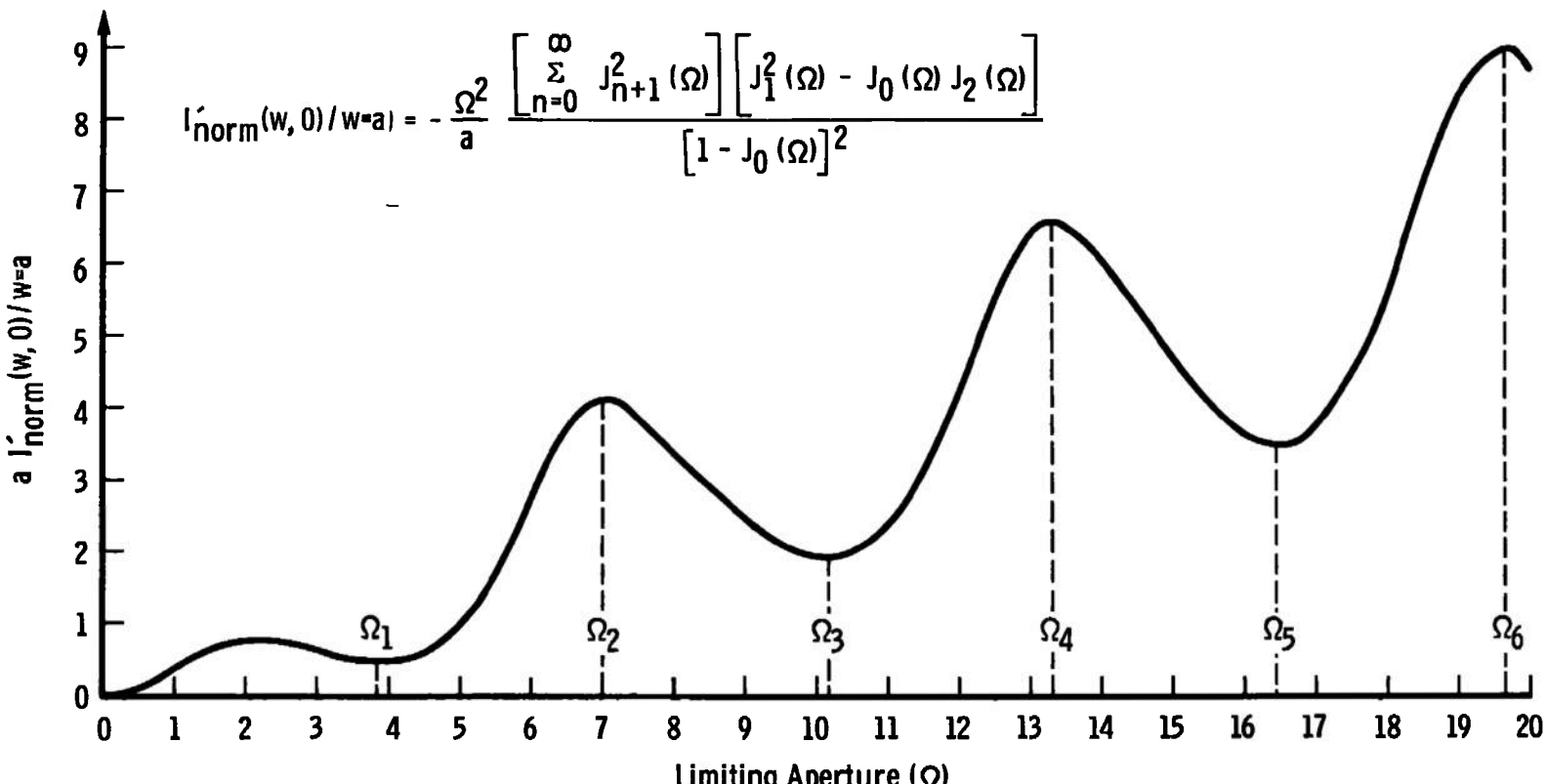

Fig. 5 Normalized Slope at the Particle Image Edge

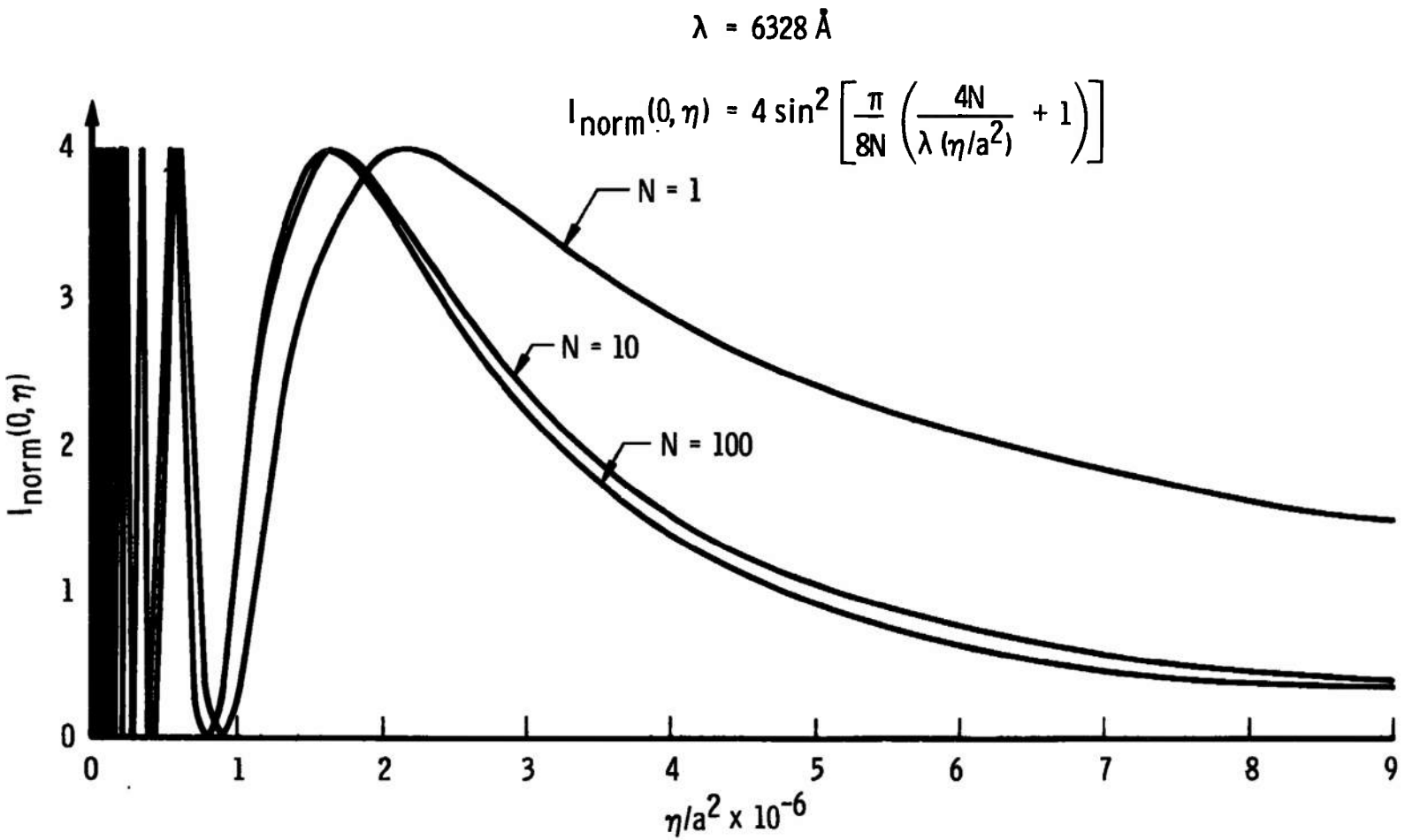

Fig. 6 Normalized Intensity Distribution along the Optic Axis

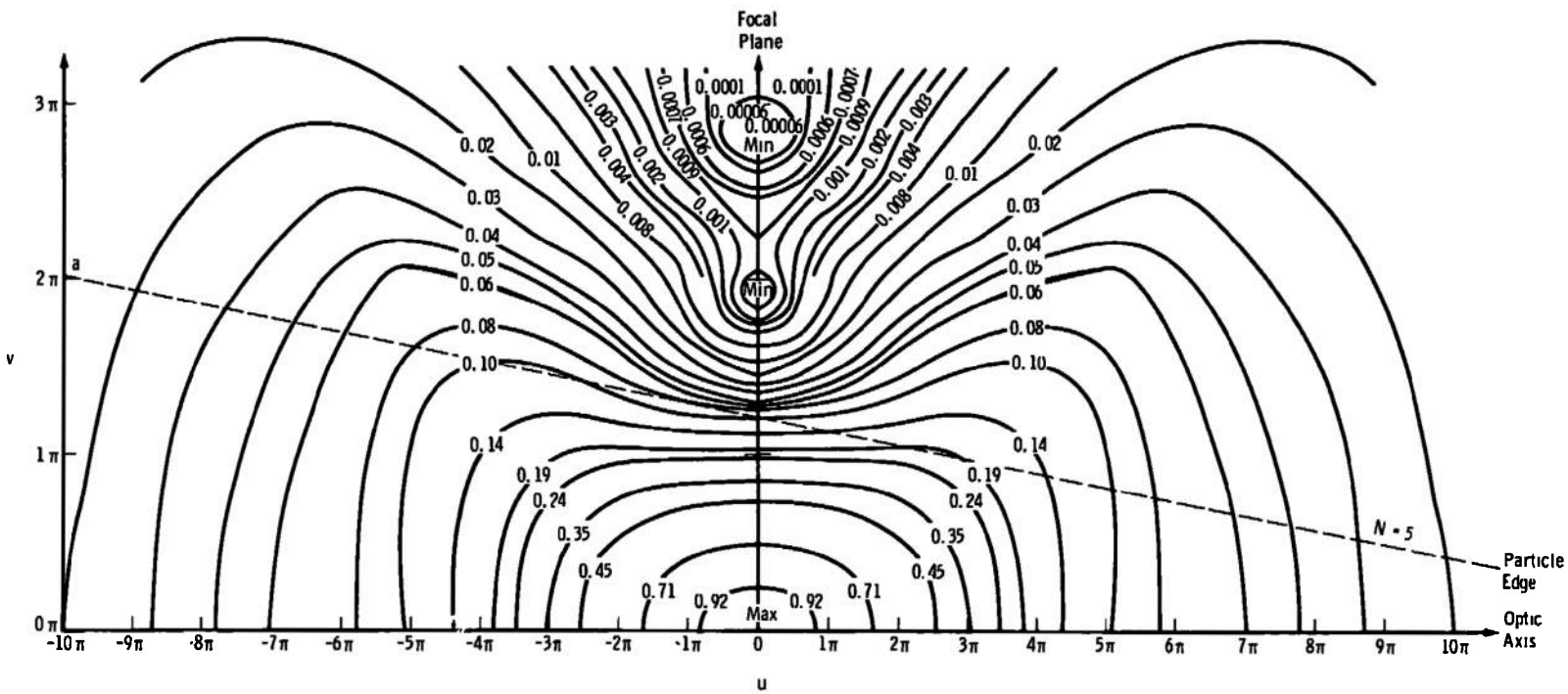

Fig. 7 Isophote Diagram

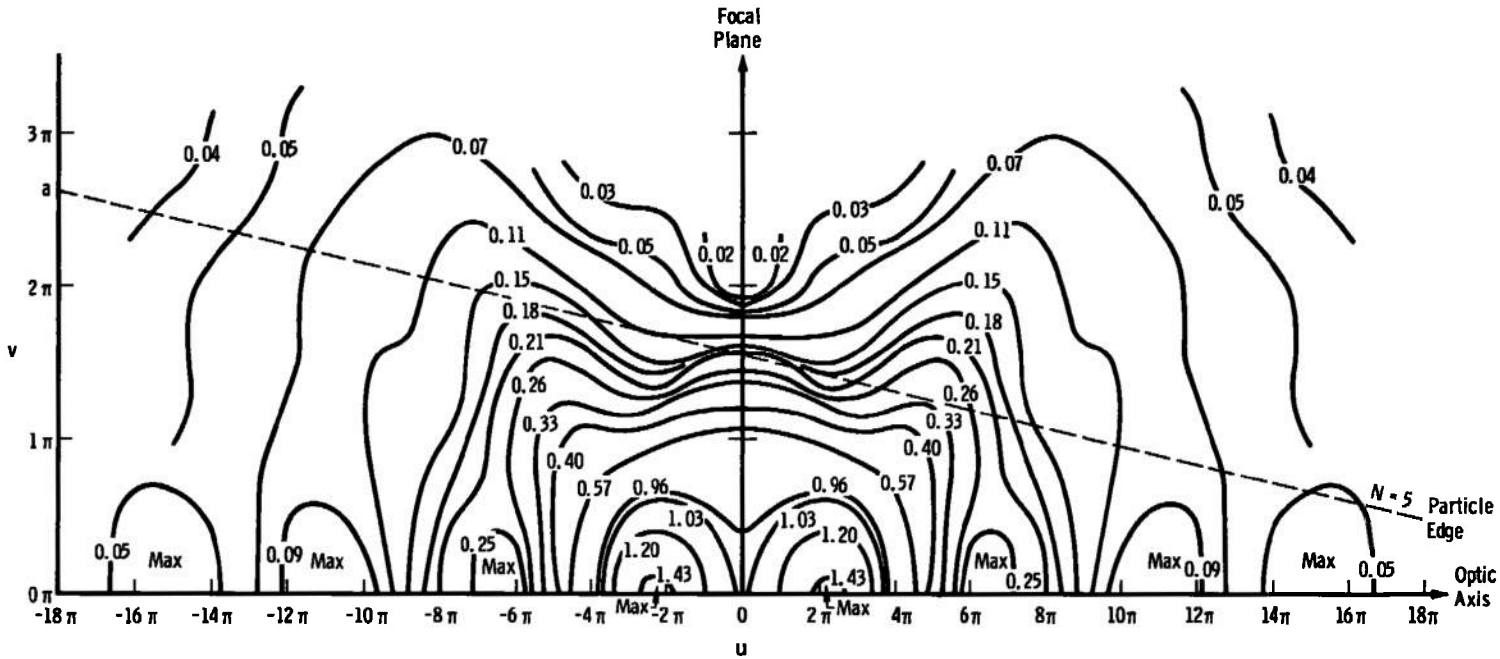

Fig. 8 Isophote Diagram

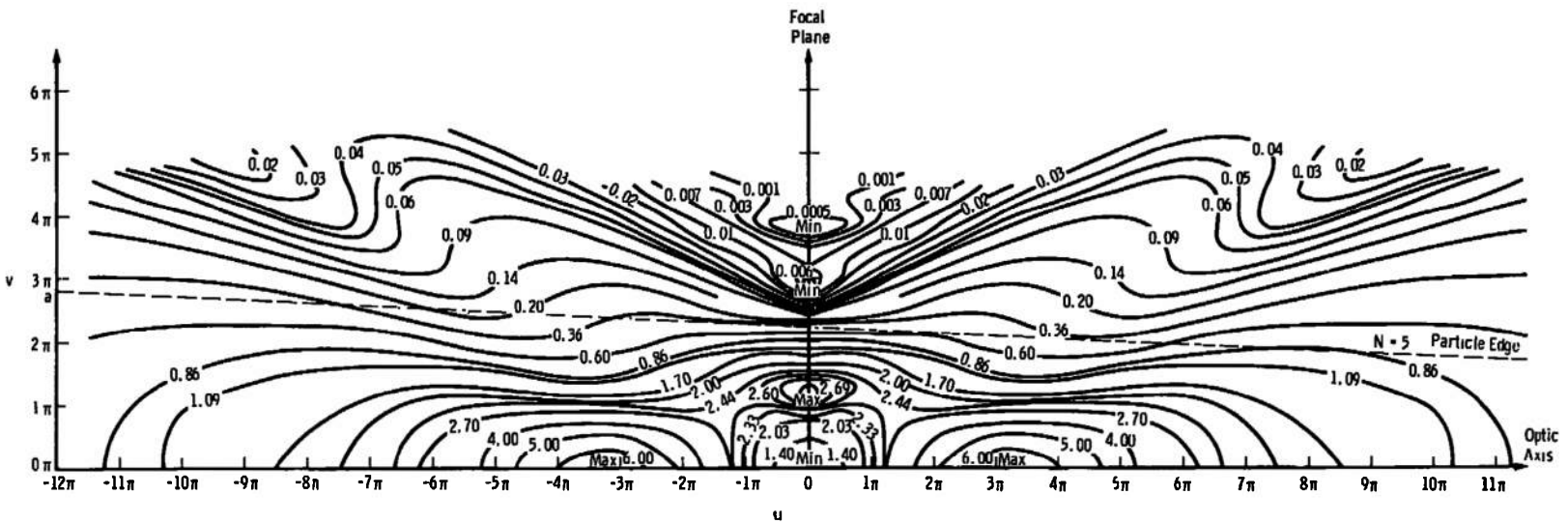

Fig. 9 Isaphote Diagram

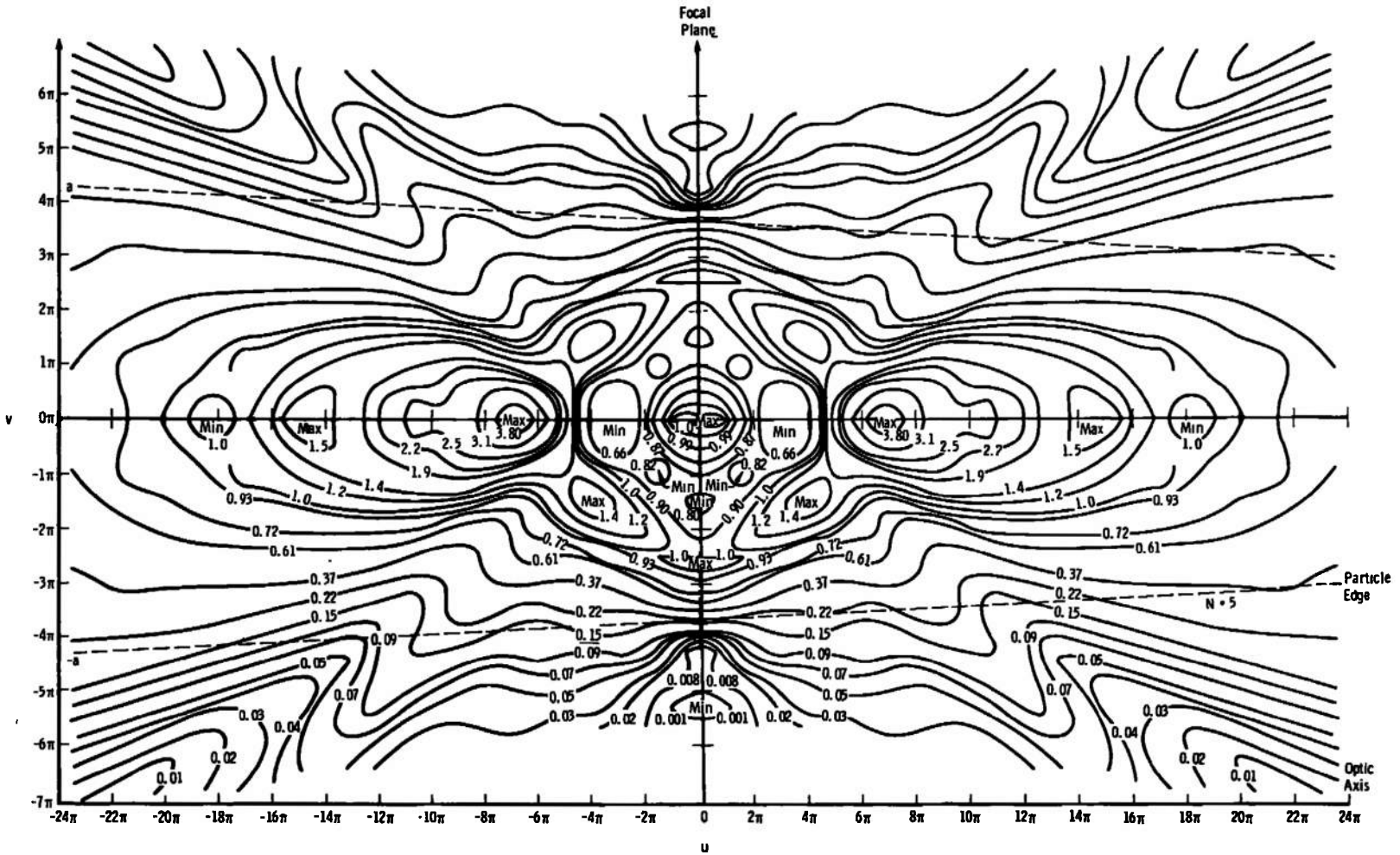

Fig. 10 Isophote Diagram

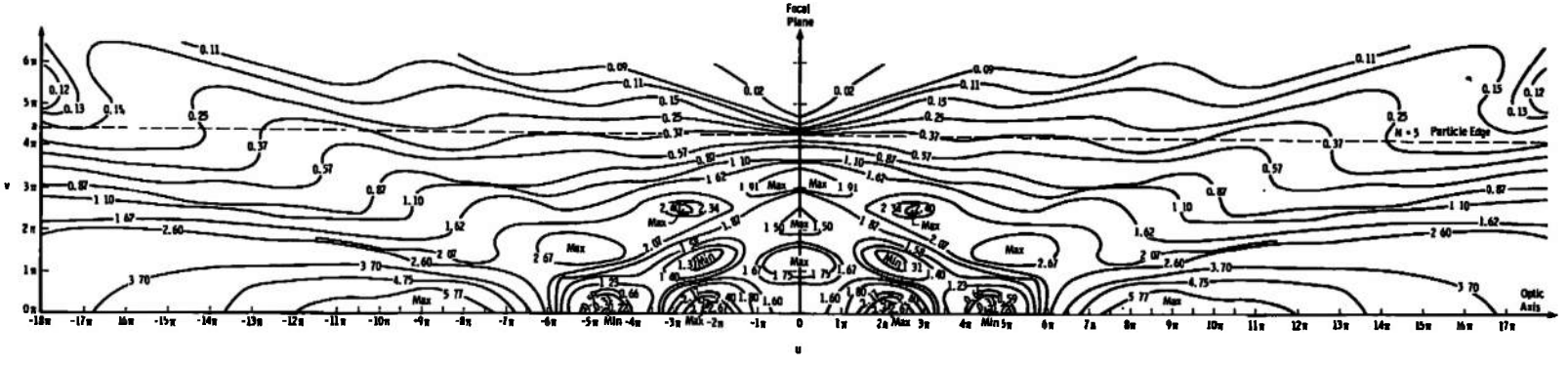

Fig. 11 Isophote Diagram

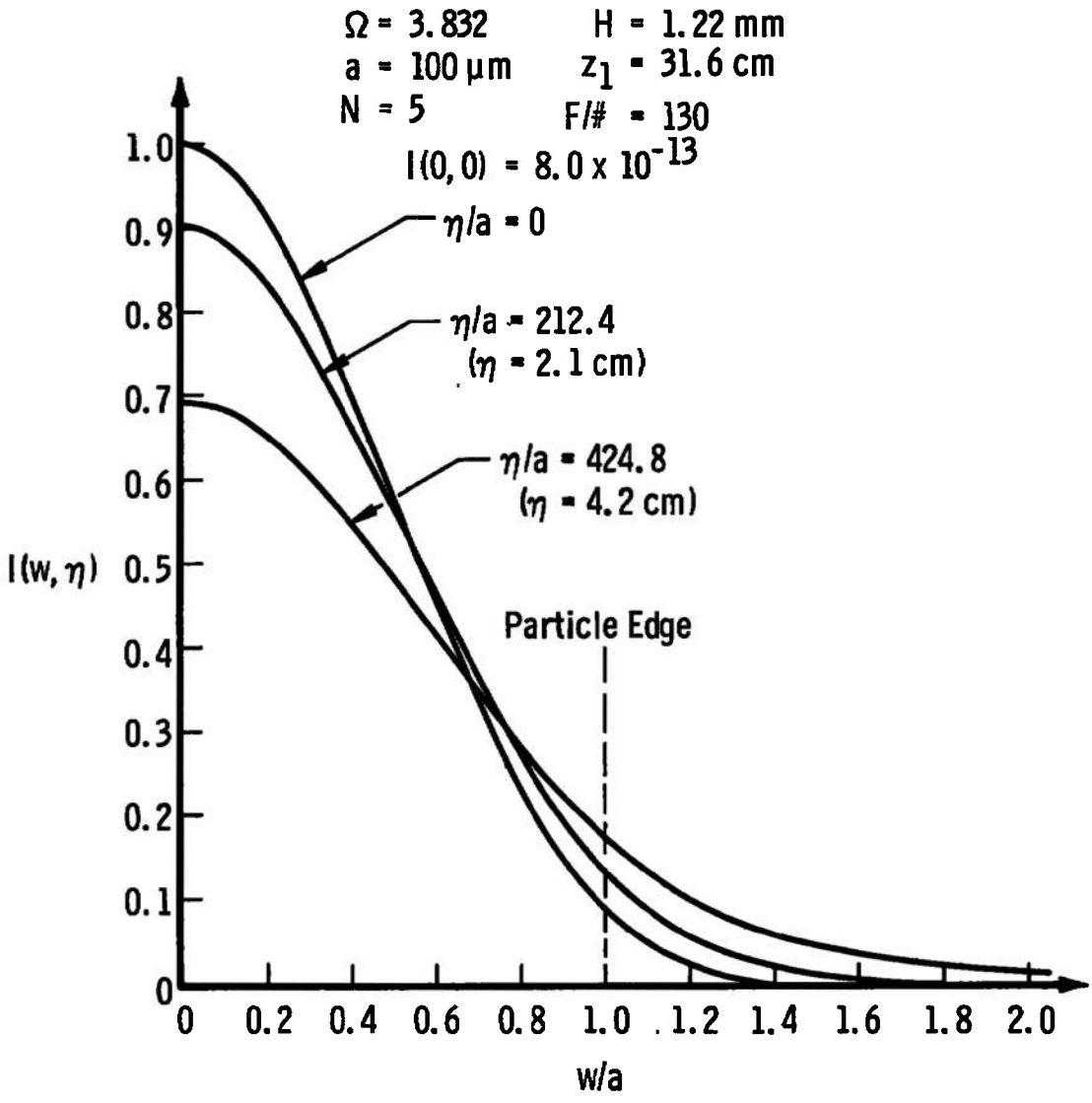

Fig. 12 Intensity Variation Perpendicular to the Optic Axis for Various Values of η

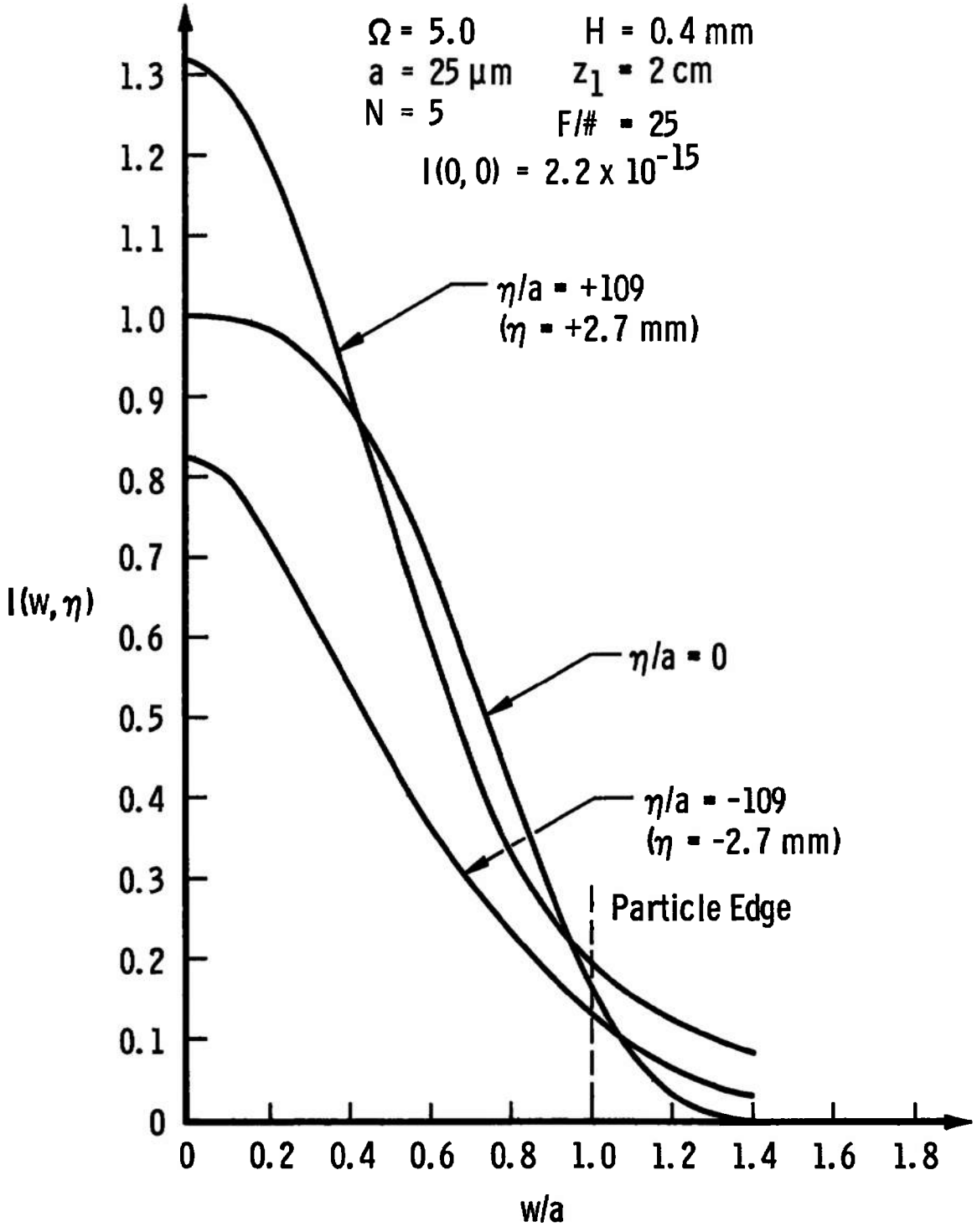

Fig. 13 Intensity Variation Perpendicular to the Optic Axis for various values of n

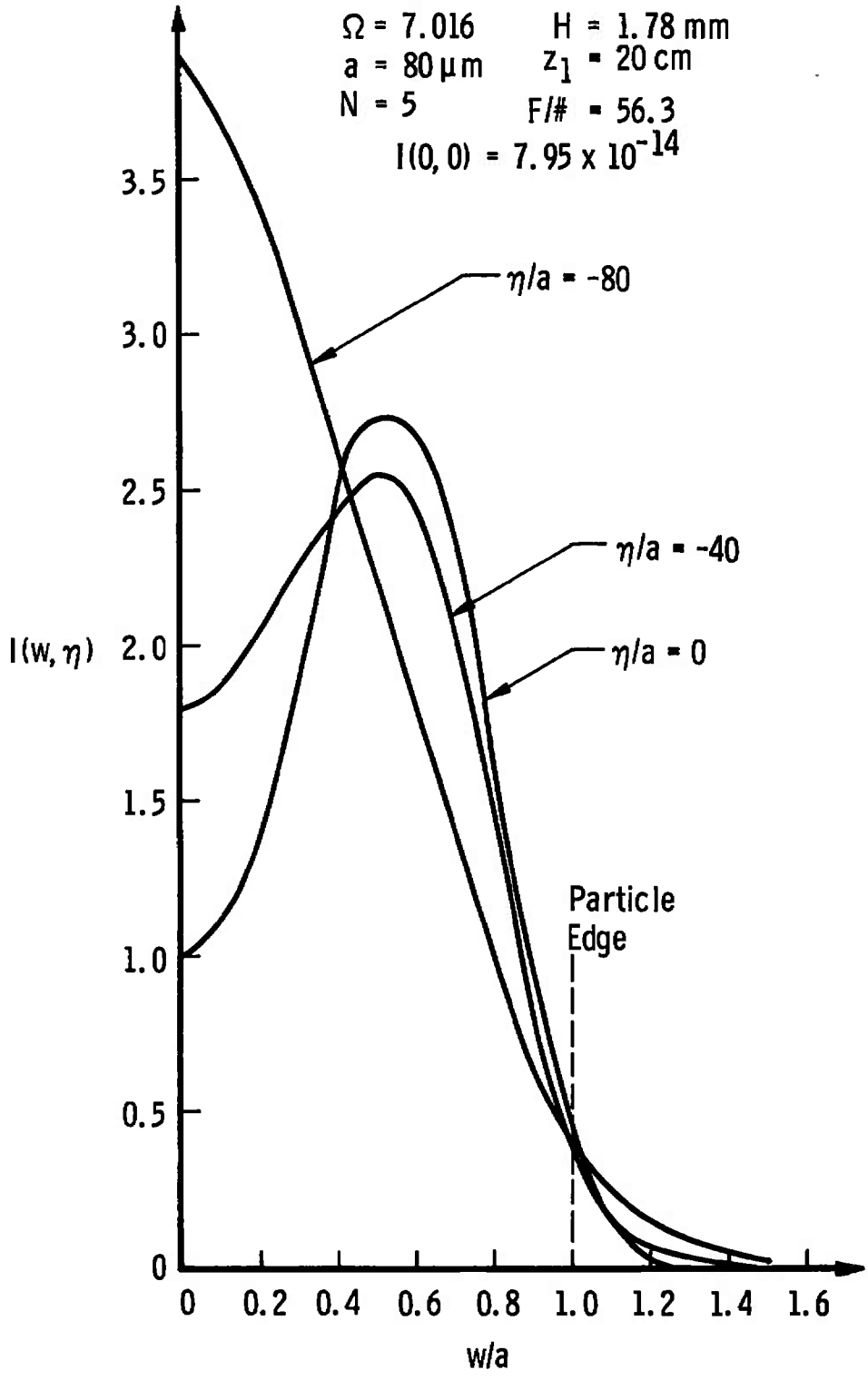

Fig. 14 Intensity Variation Perpendicular to the Optic Axis for various values of n

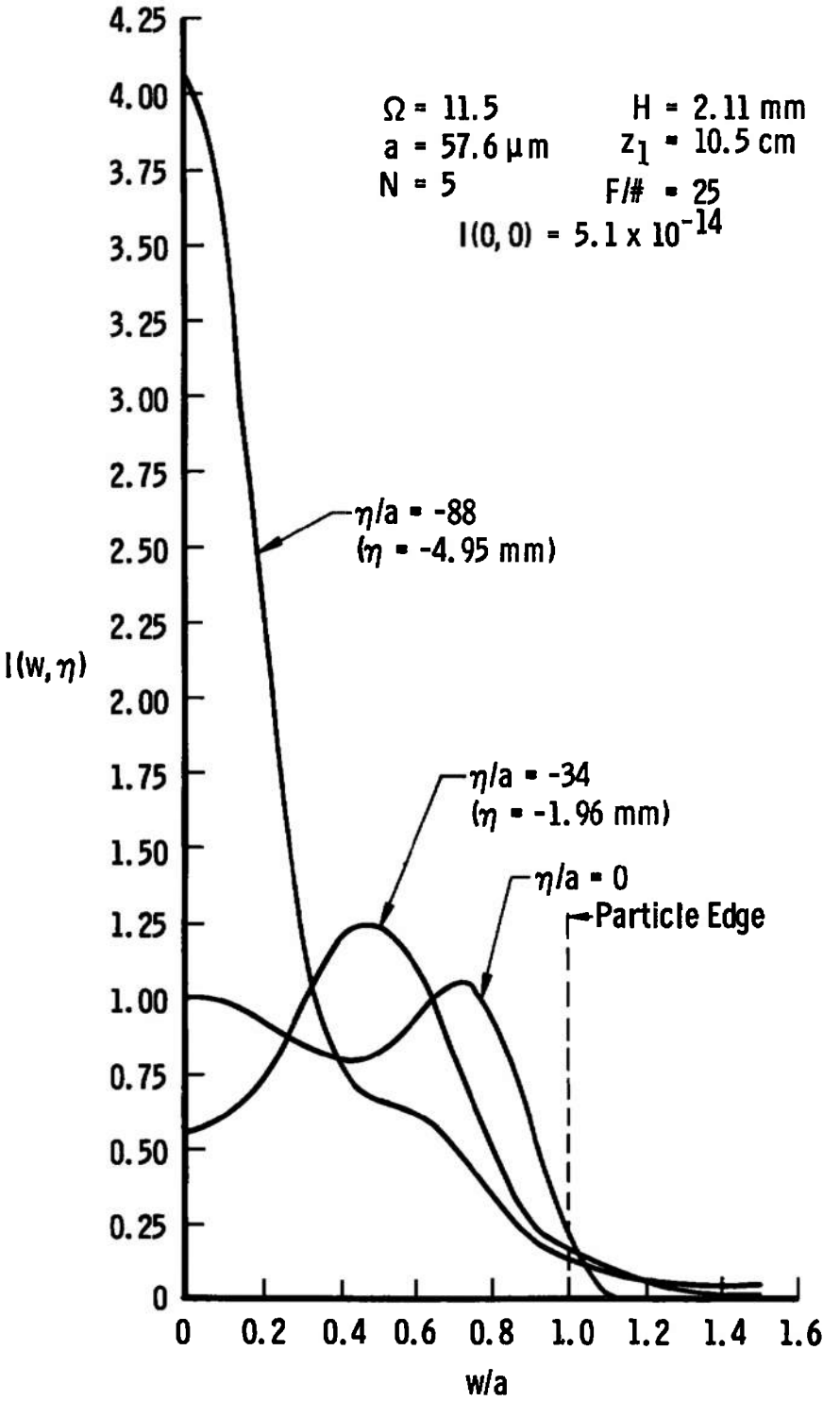

Fig. 15 Intensity Variation Perpendicular to the Optic Axis for Various Values of n

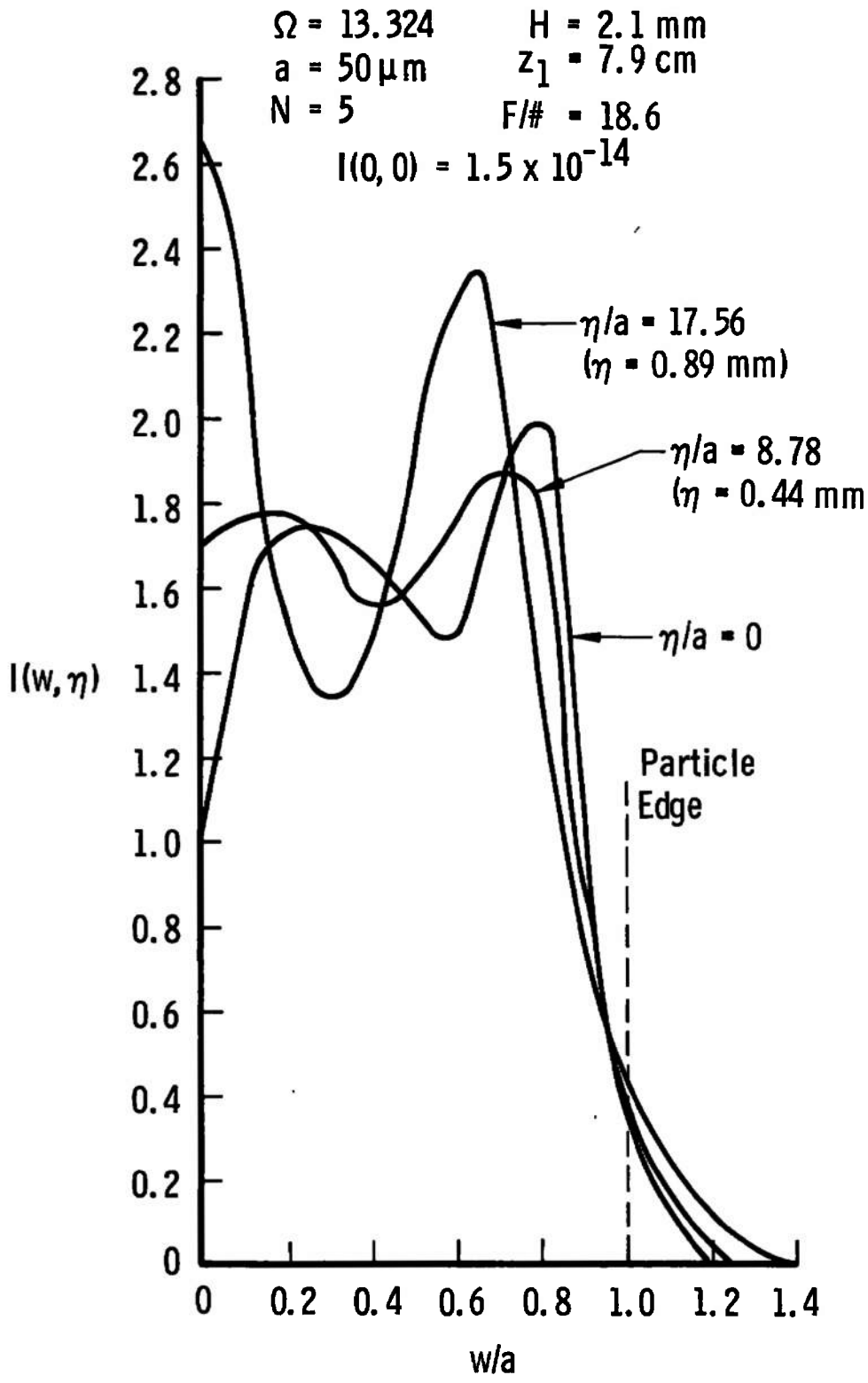

Fig. 16 Intensity Variation Perpendicular to the Optic Axis for Various Values of η

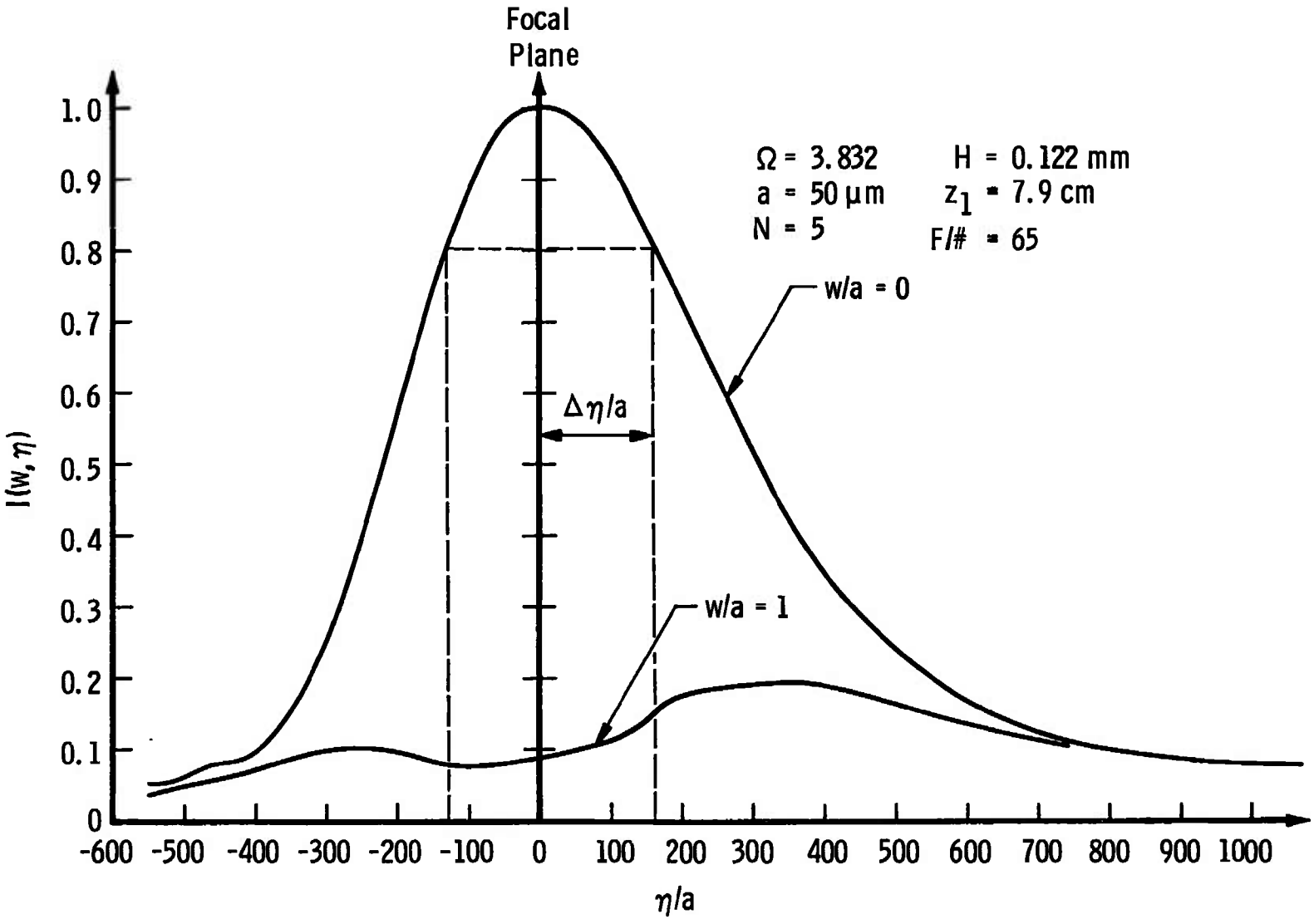

Fig. 17 Intensity Variation at the Center and Edge of the Particle Image as it is Brought into and out of Focus

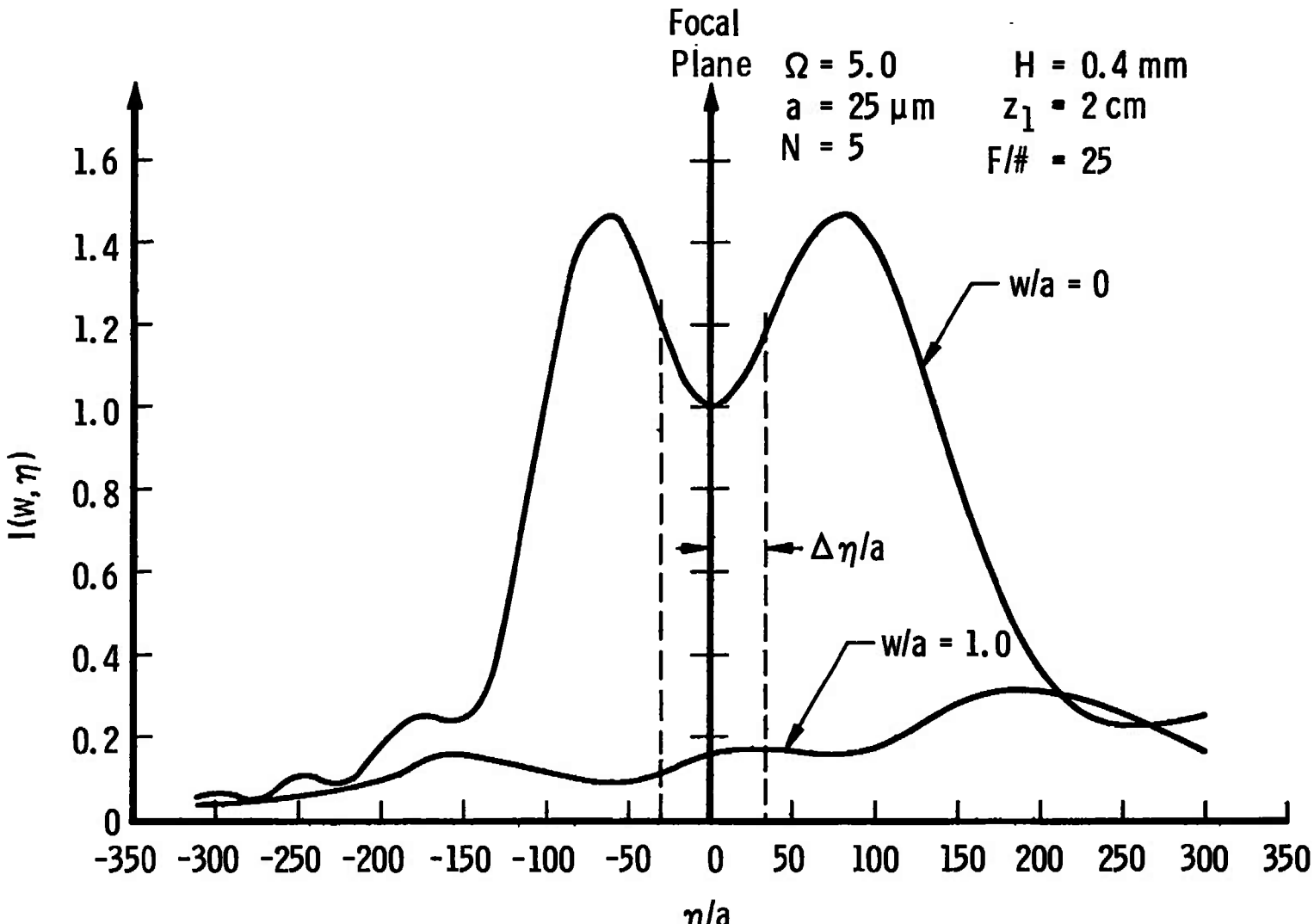

Fig. 18 Intensity Variation at the Center and Edge of the Particle Image as it is Brought into and out of Focus

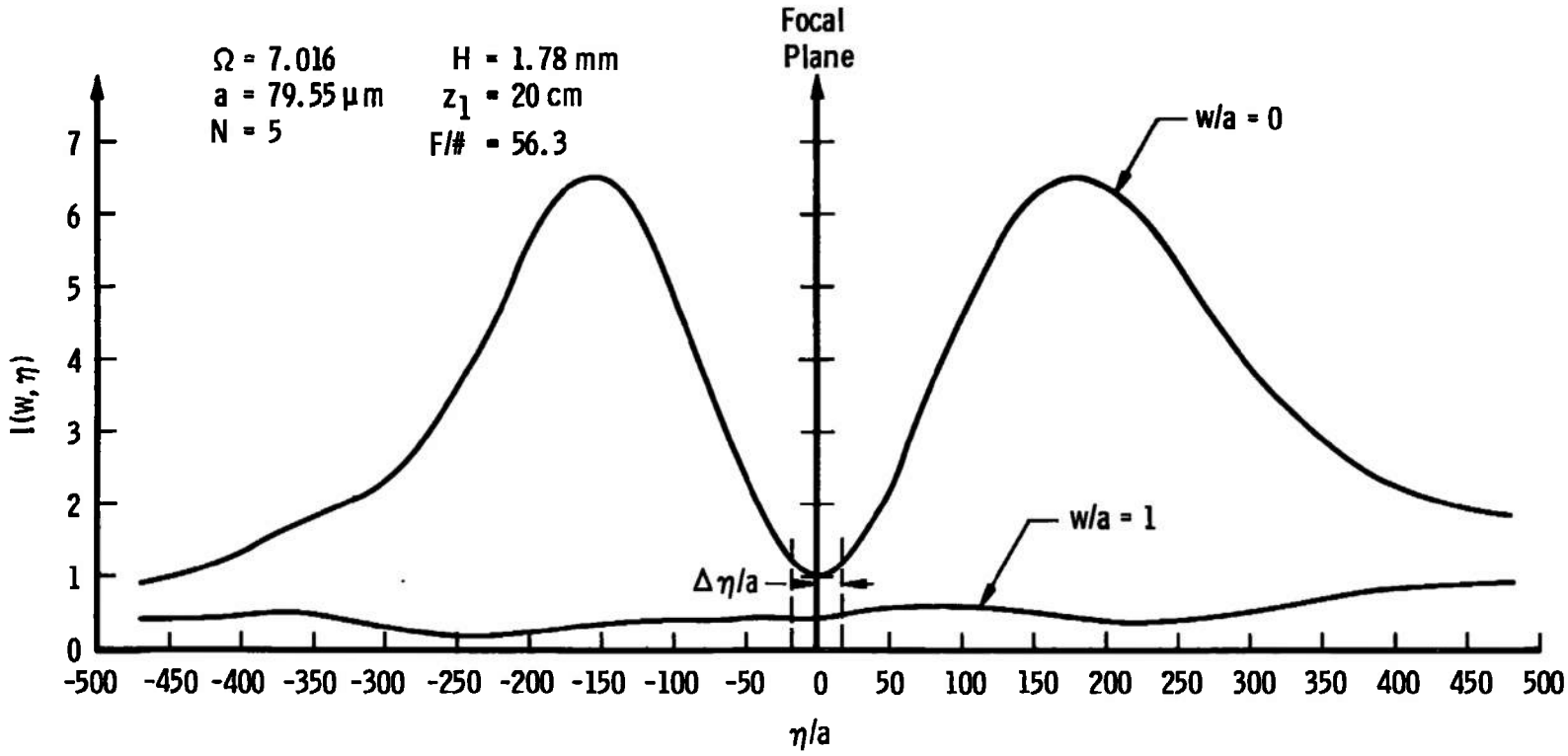

Fig. 19 Intensity Variation at the Center and Edge of the Particle Image as it is Braught into and out of Focus

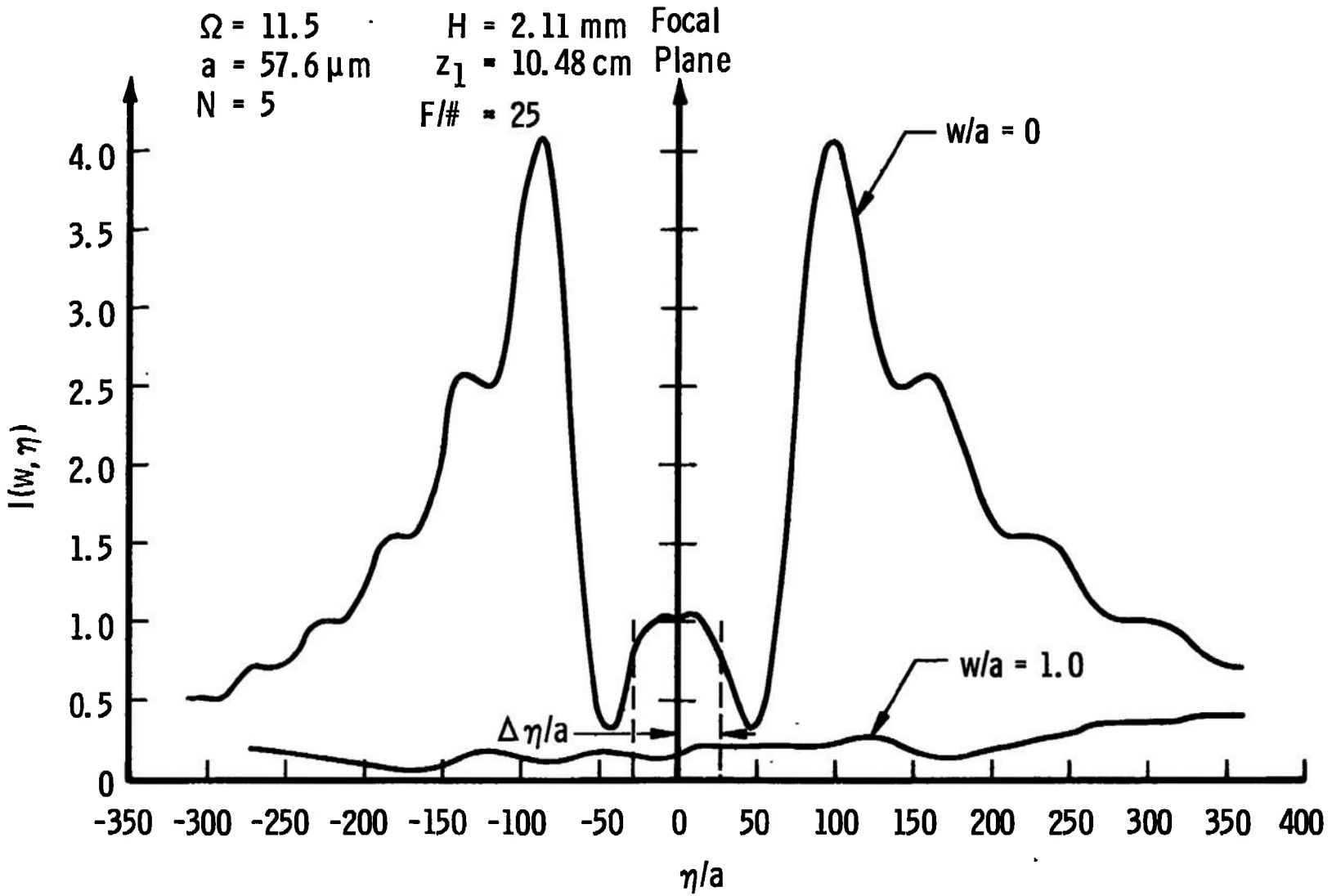

Fig. 20 Intensity Variation at the Center and Edge of the Particle Image as it is Brought into and out of Focus

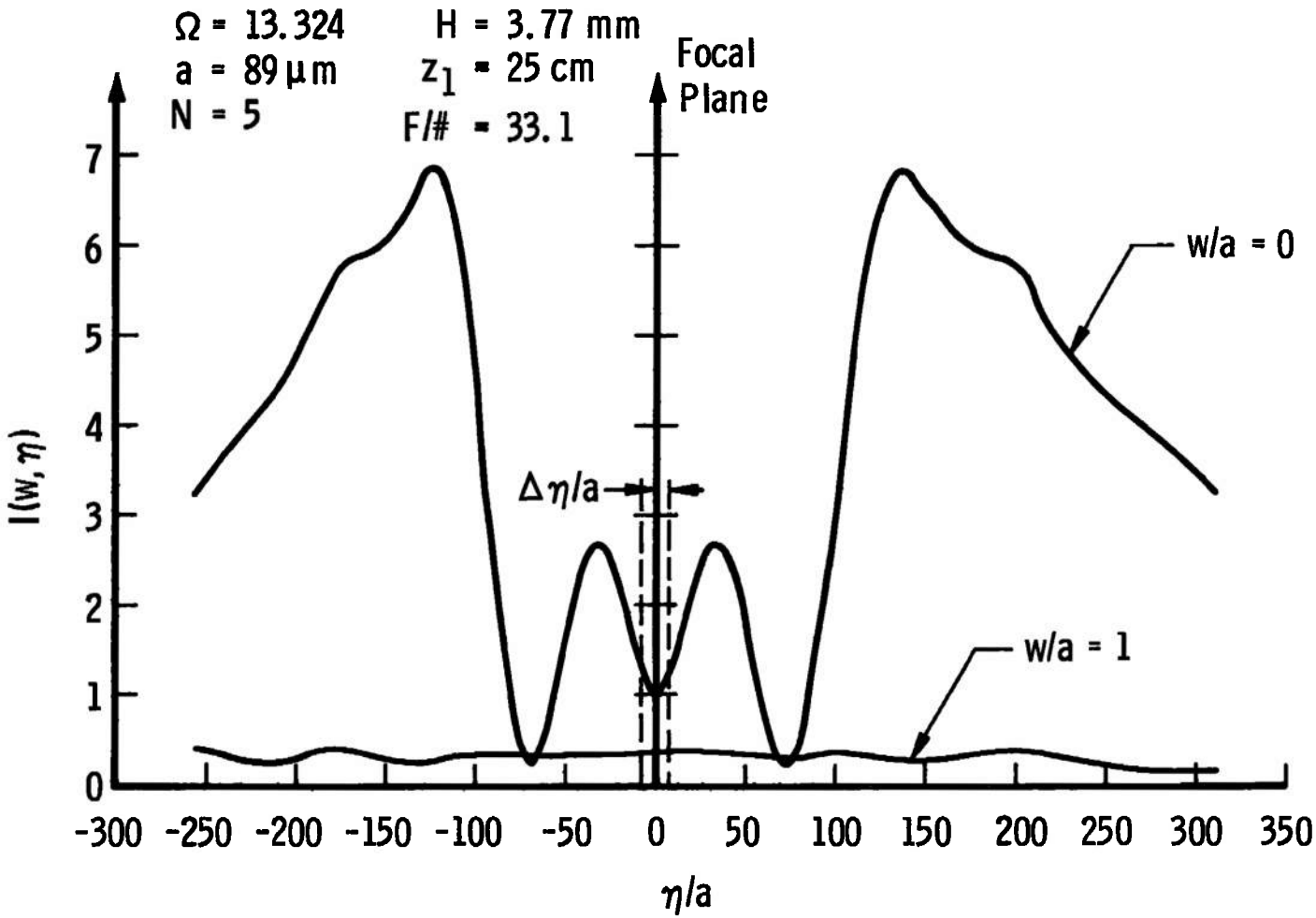

Fig. 21 Intensity Variation at the Center and Edge of the Particle Image as it is Brought into and out of Focus

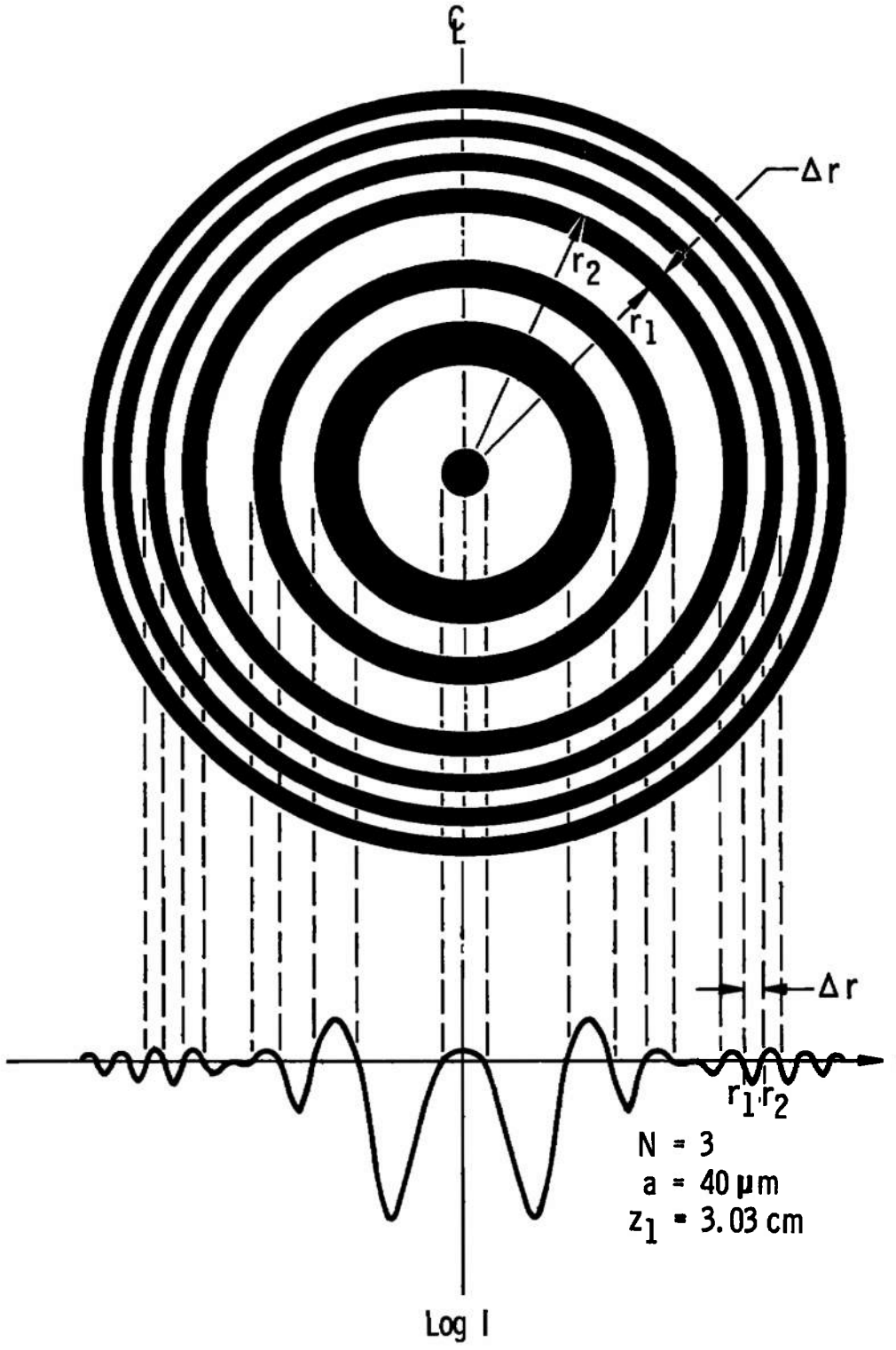

Fig. 22 The Diffraction Pattern Resulting from Plane Wave Illumination of a Circular, Opaque Particle

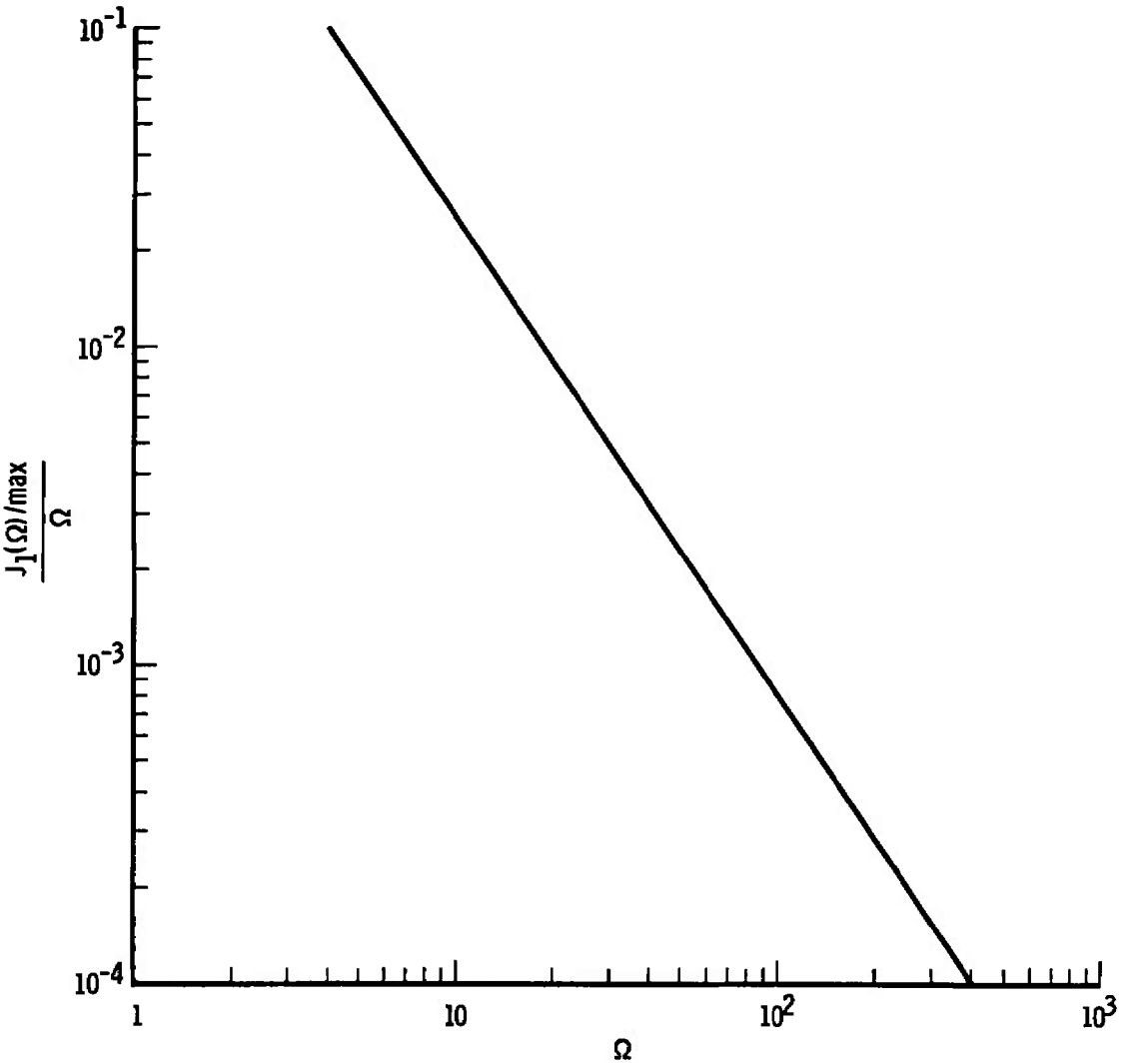

Fig. 23 Peaks of J_1 $(\Omega)/(\Omega$ versus Ω for the Signal-to-Noise Ratio Calculation

TABLE I
THEORETICAL ERROR IN THE PARTICLE RADIUS, WHEN THE INTENSITY IS 25% OF THAT AT THE CENTER OF THE IMAGE

Ω	% Error
3.832	±22.0 % Max
5.0	±8.0 %
7.016	±6.0 % Max
11.5	±1.00 %
13.324	±3.5 % Max

TABLE II
MAXIMUM THEORETICAL ERROR IN THE PARTICLE RADIUS MEASUREMENT ARISING FROM MEASURING THE OUTERMOST PEAK ON THE IMAGE

Ω	Maximum % Error
7.016	47.0 %
11.5	28.0%
13.324	19.8 %

TABLE III

FOCAL TOLERANCE CONSTANT, $K(\Omega)$, FOR A HOLOGRAM AND A THIN-LENS

Ω	$\left\lvert \Delta \left(\frac{u}{\pi}\right) \right\rvert_{20\%}$	$\left\lvert K_{holo}(\Omega) \right\rvert_{20\%}$	$K_{T.L.}(\Omega)$	$\left\lvert K_{holo}(\Omega) \right\rvert_{1st\ Extreme}$
3.832	1.33	1.79	1.37	--
5.000	1.00	0.79	0.804	1.69
7.016	0.40	0.161	0.409	1.29
11.500	2.00	0.298	0.152	0.51
13.324	1.075	0.119	0.113	0.242

TABLE IV

MAXIMUM LIMITING APERTURE RADII AND MAXIMUM ARGUMENTS OF $J_1(\Omega)$ FOR ν_{max} = 200 LINES/MM

a(μm)	Ω_{max}
10	12.6
50	62.8
100	125.7
250	314.2

r_{max}

N \ a	10 μm	50 μm	100 μm	250 μm
1	80 μm	2 mm	8 mm	5 cm
5	400 μm	1 cm	4 cm	25 cm
10	800 μm	2 cm	8 cm	50 cm
20	1.6 mm	4 cm	16 cm	1 m
50	4 mm	10 cm	40 cm	---
80	6.4 mm	16 cm	64 cm	---
100	8 mm	20 cm	80 cm	---

TABLE V
MAXIMUM LIMITING APERTURE RADII AND MAXIMUM ARGUMENTS OF $J_1(\Omega)$ FOR THE DIFFRACTION PATTERN RECORDING LIMITED BY FILM NOISE

	a = 10 μm		a = 50 μm		a = 100 μm		a = 250 μm	
N	Ω_{max}	r_{max}(mm)	Ω_{max}	r_{max}(mm)	Ω_{max}	r_{max}(mm)	Ω_{max}	r_{max}(cm)
1	41	0.26	122	3.88	195	12.42	360	5.73
5	24	0.764	70	11.15	114	36.3	208	16.55
10	19	1.21	56	17.82	90	57.4	165	26.3
20	15	1.91	45	28.6	70	89.1	130	41.4
50	11	3.5	33	52.5	52	166.0	96	76.4
80	9.5	4.84	28	71.4	44.5	226.5	82	104.4
100	8.8	5.6	26	82.8	41	261.0	77	122.5

SNR = 1

APPENDIX III
COMPUTER PROGRAM FOR THE FOCUSING INTEGRAL

```
FORTRAN IV G LEVEL 1, MOD 3            MAIN              DATE = 70019        21/06/35            PAGE 0001

0001              IMPLICIT REAL*8 (A-H,O-Z)
0002              REAL*4 XMIN,XMAX,DELTAX,YMIN,YMAX,DELTAY
0003              COMMON/KOUNT/ NE,NW
0004              COMMON/INPUT/ XMIN,XMAX,DELTAX,YMIN,YMAX,DELTAY,INDMX,INO
0005              COMMON  /ALL/  W,O,BL,FK,Z
0006              COMMON  /ONETA/ ETA
0007              ICOUNT=0
0008          385 CALL ERRSET(207,256,5,1)
0009              READ (5,1000)  Z,ALAM,GAM,CAPN
0010              READ(5,1000)WM,WMAX,WDEL,RLOWER
0011              READ(5,1000)ETAM,ETAX,ETAD,CODE
0012              PI= 3.14159265359
0013              A=   ALAM * Z
0014              A=  A/ (4.0 * CAPN)
0015              A= DSQRT(A)
0016              WRITE(6,1020) Z,ALAM,GAM,CAPN
0017         1020 FORMAT (1H1,'     Z= ',E20.8,'   LAMBDA= ',E20.8,/,
                 1'      GAMMA= ',E20.8,'  N= ',F20.8)
0018              BL=1.0
0019              FK= 2.*PI/ALAM
0020              FETA = ETAM * A
0021              FINETA= ETAX* A
0022              DELETA = ETAD * A
0023              FW  = WM * A
0024              FINW = WMAX * A
0025              DELW =  WDEL * A
0026              H=(GAM/PI)*DSQRT(Z*ALAM*CAPN)
0027              FNO= PI/(2.0*GAM) * DSQRT( Z/(CAPN*ALAM))
0028              WRITE(6,1021)A,FNO,RLOWER,H
0029         1021 FORMAT(1H0,' A= ',E20.8,' F#= ',F20.8,' LOWER= ',E20.8,' H= ',
                 *E20.8)
0030              TERM = ALAM*Z* CAPN
0031              C =  2.0 *DSQRT(TERM)
0032              D =  PI  / DSQRT(TERM)
0033              FIE= (ETAX-ETAM)/ ETAD
0034              FIW= (WMAX-WM)/WDEL
0035              NW = FIW +1.0
0036              NE = FIE +1.0
0037              XMIN= ETAM
0038              XMAX= ETAX
0039              DELTAX= ETAD
0040              YMIN=  WM
0041              YMAX=  WMAX
0042              DELTAY =  WDEL
0043              ETA=0.0
0044              W=0.0
0045              IF(CODE.EQ.96.)GO TO 69
0046              CALL GSS32(I,RLOWER,H,E1)
```

```
//ARD01549  JOB (ARO,                                                    *
//              SRS00452,01,BC5916),' B322 P/O 020',MSGLEVEL=1,          *
//              CLASS=C
//        EXEC FTGLNKGO,MCHLIST=LIST
XX        PROC BLKFAC=1596,DATABLK=400,PLOTLIB=PLOT835,MCHLIST=NOLIST
XXFTG     EXEC  PGM=IEYFORT,PARM='SOURCE,MAP,&MCHLIST'
XXSYSLIN DD UNIT=WORK,DISP=(,PASS),SPACE=(CYL,(3,1)),                    *
XX              DCB=(RECFM=FB,LRECL=80,BLKSIZE=3200)
XXSYSPRINT DD SYSOUT=A,UNIT=PRINT,SPACE=(1200,(700,100),RLSE,,ROUND),   *
XX              DCB=(RECFM=FBA,LRECL=120,BLKSIZE=1200)
//SYSIN DD *
IEF236I ALLOC. FOR ARD01549 FTG
IEF237I SYSLIN   ON 130
IEF237I SYSPRINT ON 136
IEF237I SYSIN    ON 131
```

```
0047              CALL GSS32(2,RLOWER,H,E2)
0048              GO TO 6969
0049           69 CALL GSS96(1,RLOWER,H,E1)
0050              CALL GSS96(2,RLOWER,H,E2)
0051         6969 CONTINUE
0052              ETAN= C**2 * (E1**2 + E2**2)
0053              WRITE (6,1010)  ETAN
0054         1010 FORMAT (1H0,'  I(0,0) = ',E20.8)
0055              W = FW - DELW
0056              ETA=FETA- DELETA
0057              DO 1  I=1,NW
0058              W=  W + DELW
0059              DO 1  J=1,NE
0060              ETA = ETA +DELETA
0061              IF  (J.EQ.1.OR.J.EQ.26.OR.J.EQ.51.OR.J.EQ.76)  CALL FLIP
0062              IF(CODE.EQ.96.)GO TO 96
0063              CALL GSS32(1,RLOWER,H,E1)
0064              CALL GSS32(2,RLOWER,H,E2)
0065              GO TO 9696
0066           96 CALL GSS96(1,RLOWER,H,E1)
0067              CALL GSS96(2,RLOWER,H,E2)
0068         9696 CONTINUE
0069              ETAI = C**2  *  (E1**2 + E2**2)
0070              VNORM= ETAI/ETAN
0071              THEW= WM+ ((I-1)*WDEL)
0072              THEETA=  ETAM + ((J-1)*ETAD)
0073              WRITE(6,1002)THEW,THEETA,VNORM
0074              PHI=DATAN2(E2,E1)
0075              AMAG=DSQRT(E1**2+E2**2)
0076              WRITE(6,2000)AMAG,PHI
0077         2000 FORMAT(25X,'MAGNITUDE=',E15.8,5X,'ANGLE(RADIANS)=',E15.8)
0078              IF (J.EQ.NE)   ETA= FETA-DELETA
0079            1 CONTINUE
0080         1000 FORMAT (4E15.0)
0081         1002 FORMAT  (20X,3E20.8)
0082              ICOUNT=ICOUNT+1
0083              IF(ICOUNT.EQ.1)WRITE(6,11111)
0084        11111 FORMAT(//,'   RUN FOR GSS96 FOLLOWS   ',//)
0085              IF(ICOUNT.EQ.1)GO TO 385
0086              STOP
0087              END
```

```
FORTRAN IV G LEVEL 1, MOD 3          MAIN          DATE = 70019          21/06/35          PAGE 0003

                    COMMON BLOCK /KOUNT    / MAP SIZE      8
SYMBOL    LOCATION    SYMBOL    LOCATION    SYMBOL    LOCATION    SYMBOL    LOCATION    SYMBOL    LOCATION
NE            0       NW            4

                    COMMON BLOCK /INPUT    / MAP SIZE     20
SYMBOL    LOCATION    SYMBOL    LOCATION    SYMBOL    LOCATION    SYMBOL    LOCATION    SYMBOL    LOCATION
XMIN          0       XMAX          4       DELTAX        8       YMIN          C       YMAX         10
DELTAY       14       INDMX        18       IND          1C

                    COMMON BLOCK /ALL      / MAP SIZE     28
SYMBOL    LOCATION    SYMBOL    LOCATION    SYMBOL    LOCATION    SYMBOL    LOCATION    SYMBOL    LOCATION
W             0       D             8       BL           10       FK           18       Z            20

                    COMMON BLOCK /DNETA    / MAP SIZE      8
SYMBOL    LOCATION    SYMBOL    LOCATION    SYMBOL    LOCATION    SYMBOL    LOCATION    SYMBOL    LOCATION
ETA           0

                    SUBPROGRAMS CALLED
SYMBOL    LOCATION    SYMBOL    LOCATION    SYMBOL    LOCATION    SYMBOL    LOCATION    SYMBOL    LOCATION
ERRSET       E8       IBCOM#       EC       GSS32        F0       GSS96        F4       FLIP         F8
DSQRT        FC       DATAN2      100

                    SCALAR MAP
SYMBOL    LOCATION    SYMBOL    LOCATION    SYMBOL    LOCATION    SYMBOL    LOCATION    SYMBOL    LOCATION
ALAM        188       GAM         1C0       CAPN        1C8       WM          100       WMAX        108
WDEL        1E0       RLOWER      1E8       ETAM        1F0       ETAX        1F8       ETAD        200
CODE        208       PI          210       A           218       FETA        220       FINETA      228
DELETA      230       FW          238       FINW        240       DELW        248       H           250
FNO         258       TERM        260       C           268       FIE         270       FIW         278
E1          280       E2          288       ETAN        290       ETAI        298       VNORM       2A0
THEW        2A8       THEETA      280       PHI         2B8       AMAG        2C0       ICOUNT      2C8
I           2CC       J           200

                    FORMAT STATEMENT MAP
SYMBOL    LOCATION    SYMBOL    LOCATION    SYMBOL    LOCATION    SYMBOL    LOCATION    SYMBOL    LOCATION
 1020        204       1021        311       1010       33F       2000        354       1000        370
 1002        384      11111        380
```

UNCLASSIFIED
Security Classification

DOCUMENT CONTROL DATA - R & D

(Security classification of title, body of abstract and indexing annotation must be entered when the overall report is classified)

1. ORIGINATING ACTIVITY *(Corporate author)*
Arnold Engineering Development Center
ARO, Inc., Operating Contractor
Arnold Air Force Station, Tennessee 37389

2a. REPORT SECURITY CLASSIFICATION
UNCLASSIFIED

2b. GROUP
N/A

3. REPORT TITLE
RESOLUTION LIMITS OF FRAUNHOFER HOLOGRAPHY

4. DESCRIPTIVE NOTES *(Type of report and inclusive dates)*
Final Report June to September 1969

5. AUTHOR(S) *(First name, middle initial, last name)*
Ronald A. Belz, ARO, Inc.

6. REPORT DATE
May 1970

7a. TOTAL NO. OF PAGES
70

7b. NO. OF REFS
19

8a. CONTRACT OR GRANT NO.
F40600-69-C-0001

b. PROJECT NO.
4344

c. Task 32

d. Program Elements 64719F and 62201F

9a. ORIGINATOR'S REPORT NUMBER(S)
AEDC-TR-70-23

9b. OTHER REPORT NO(S) *(Any other numbers that may be assigned this report)*
N/A

10. DISTRIBUTION STATEMENT
This document has been approved for public release and sale; its distribution is unlimited.

11. SUPPLEMENTARY NOTES
Available in DDC.

12. SPONSORING MILITARY ACTIVITY
Arnold Engineering Development Center, AFSC, Arnold Air Force Station, Tennessee 37389

13. ABSTRACT
The resolution of an in-line hologram recorded with plane waves in the Fraunhofer region of a circular, opaque, particle is evaluated. From the diffraction integral for the reconstructed, real image the intensity distribution about the image is found. Criteria for determining the edge of the image in addition to determining the plane of focus are specified from the data, and the measurement accuracies are found. The inaccuracies are shown to be a result of the inability of the film to record all of the light diffracted by the particle. The reasons for this, film grain noise and its cutoff frequency and dynamic range, are explained and their relative effects compared for the various particle sizes and recording distances.

DD FORM 1 NOV 65 1473

UNCLASSIFIED
Security Classification

14. KEY WORDS	LINK A ROLE	LINK A WT	LINK B ROLE	LINK B WT	LINK C ROLE	LINK C WT
holography						
holograms						
photographic film						
optical interferometers						
optical measurement						
diffraction						